STATISTICAL PROPERTIES OF WAVE CREST LENGTHS IN HURRICANE GENERATED SEAS

FDOT CONTRACT NUMBER: BDT63

FINAL REPORT

PREPARED BY

OEA A DIVISION OF INTERA

HÜSEYIN DEMIR, D. MAX SHEPPARD

100 SW 75TH STREET, SUITE 107

GAINESVILLE, FL 32607

PREPARED FOR

FLORIDA DEPARTMENT OF TRANSPORTATION

JUNE 2013

DISCLAIMER

The opinions, findings, and conclusions expressed in this publication are those of the authors and not necessarily those of the State of Florida Department of Transportation

METRIC CONVERSION TABLE

SYMBOL	WHEN YOU KNOW	MULTIPLY BY	TO FIND	SYMBOL
LENGTH				
in	inches	25.4	millimeters	mm
ft	feet	0.305	meters	m
yd	yards	0.914	meters	m
mi	miles	1.61	kilometers	km
AREA				
in^2	square inches	645.2	square millimeters	mm^2
ft^2	square feet	0.093	square meters	m^2
yd^2	square yard	0.836	square meters	m^2
ac	acres	0.405	hectares	ha
mi^2	square miles	2.59	square kilometers	km^2
VOLUME				
fl oz	fluid ounces	29.57	milliliters	mL
gal	gallons	3.785	liters	L
ft^3	cubic feet	0.028	cubic meters	m^3
yd^3	cubic yards	0.765	cubic meters	m^3
NOTE: volumes greater than 1000 L shall be shown in m^3				
MASS				
oz	ounces	28.35	grams	g
lb	pounds	0.454	kilograms	kg
T	short tons (2000 lb)	0.907	megagrams (or "metric ton")	Mg (or "t")
TEMPERATURE (exact degrees)				
^oF	Fahrenheit	5 (F-32)/9 or (F-32)/1.8	Celsius	^oC
ILLUMINATION				
fc	foot-candles	10.76	lux	lx
fl	foot-Lamberts	3.426	$candela/m^2$	cd/m^2
FORCE and PRESSURE or STRESS				
lbf	poundforce	4.45	newtons	N
lbf/in^2	poundforce per square inch	6.89	kilopascals	kPa
LENGTH				
mm	millimeters	0.039	inches	in
m	meters	3.28	feet	ft
SYMBOL	**WHEN YOU KNOW**	**MULTIPLY BY**	**TO FIND**	**SYMBOL**
LENGTH				
m	meters	1.09	yards	yd
km	kilometers	0.621	miles	mi
AREA				
mm^2	square millimeters	0.0016	square inches	in^2
m^2	square meters	10.764	square feet	ft^2
m^2	square meters	1.195	square yards	yd^2
ha	hectares	2.47	acres	ac
km^2	square kilometers	0.386	square miles	mi^2
VOLUME				
mL	milliliters	0.034	fluid ounces	fl oz
L	liters	0.264	gallons	gal
m^3	cubic meters	35.314	cubic feet	ft^3

m^3	cubic meters	1.307	cubic yards	yd^3
MASS				
g	grams	0.035	ounces	oz
kg	kilograms	2.202	pounds	lb
Mg (or "t")	megagrams (or "metric ton")	1.103	short tons (2000 lb)	T
TEMPERATURE (exact degrees)				
^oC	Celsius	1.8C+32	Fahrenheit	^oF
ILLUMINATION				
lx	lux	0.0929	foot-candles	fc
cd/m^2	$candela/m^2$	0.2919	foot-Lamberts	fl
FORCE and PRESSURE or STRESS				
N	newtons	0.225	poundforce	lbf
kPa	kilopascals	0.145	poundforce per square inch	lbf/in^2

Technical Report Documentation Page

1. Report No.	2. Government Accession No.	3. Recipient's Catalog No.
4. Title and Subtitle Statistical Properties of Wave Crest Lengths in Hurricane Generated Seas		5. Report Date June 2013
		6. Performing Organization Code
7. Author(s) Huseyin Demir, D. Max Sheppard		8. Performing Organization Report No.
9. Performing Organization Name and Address OEA a Division of INTERA 100 SW 75th Street, Suite 107 Gainesville, FL 32607		10. Work Unit No. (TRAIS)
		11. Contract or Grant No. BDT63
12. Sponsoring Agency Name and Address Florida Department of Transportation 605 Suwannee Street, MS 30 Tallahassee, FL 32399		13. Type of Report and Period Covered Final Report
		14. Sponsoring Agency Code
15. Supplementary Notes		

16. Abstract

The purpose of this study was to investigate wind wave crest lengths in coastal waters during tropical storm and hurricane conditions. The wave crest length is the length of the wave crest in the direction normal to the wave propagation direction. This information is needed for the computation of wave loads on bridge superstructures, fishing piers and similar structures.

Wave forces on bridge superstructures are dependent of the variation in design wave crest height over the length of the bridge span. In the AASHTO code, it is assumed that the wave crest elevation is unchanged and extends the length of the span regardless of the span length. A method for accounting for wave crest variation and its impact on wave forces on bridge spans was developed. This method takes into consideration both the length of the span and the distance between the storm water and the span low-chord elevations. Methodologies for obtaining design wave height and period based on the met/ocean information that is available is presented. When directional wave spectra for the major storms that have impacted the location of interest are available (e.g., a Level III met/ocean analysis has been performed and the spectra saved), more accurate design wave heights and periods can be obtained. For situations where wave spectra are not available (Level I met/ocean analysis), conservative values for the spectral parameters must be used that result in conservative force estimates. The forces calculated using this methodology may significantly decrease the predicted wave forces on bridge superstructures.

17. Key Word		18. Distribution Statement	
Wave, crest, wave crest length, hurricane, bridges, wave forces, superstructures, statistics		No restrictions.	
19. Security Classif. (of this report)	20. Security Classif. (of this page)	21. No. of Pages	22. Price
Unclassified.	Unclassified.	66	

Executive Summary

The purpose of this study was to investigate wind wave crest lengths in coastal waters during tropical storm and hurricane conditions. The wave crest length is the length of the wave crest in the direction normal to the wave propagation direction. This information is needed for the computation of wave loads on bridge superstructures, fishing piers and similar structures.

The literature and data search uncovered a number of interesting technical papers on the subject and three measured data sets. The pertinent papers are summarized in this report. The data sets, however, are for offshore, deep water conditions which are of limited value to this project. One researcher, Monaldo (2000) extracted wave crest lengths from measured sea surface images under hurricane conditions and compared them to crest lengths extracted from synthetically generated sea surfaces using measured directional wave spectra from the site. The crest lengths obtained from the synthetically generated sea surfaces were, for the most part, less than those obtained from the measured sea surfaces. The interest in synthetically generated sea surfaces is due to the fact that measured sea surface image data in coastal waters under storm conditions could not be located. There are, however, directional wave spectra, produced by computer wave models such as SWAN, from several locations in coastal waters during storm conditions, from which synthetic sea surfaces can be generated.

Since the water surface varies in height along the crest, a threshold elevation is required to define the crest length. Using the storm water elevation would not be meaningful for this application since the wave forces imparted to the structure are very sensitive to the distance between the water surface and the bottom (low-chord) of the structure. Attempts to establish a procedure for arriving at a meaningful threshold value were not successful. The arbitrariness of such a selection led to the development a different approach which was successful. This approach eliminated the need to define a threshold value and in addition accounts for the crest height variation along the structure for waves approaching normal to the structure.

Most design wave heights are arrived at via predicted significant wave heights. In the AASHTO code "*Guide Specification for Bridges Vulnerable to Coastal Storms"* the design wave height is 1.8 times the design significant wave height (subject to depth and steepness limitations). The method developed in this study to account for wave crest lengths modifies the 1.8 multiplier based on the values of the span length, wave length, clearance, and directional spreading of the waves.

Table of Contents

List of Figures

List of Tables

1.0 Introduction

Wave crest lengths in a storm-generated sea have received little attention by researchers in the past due, primarily, to the lack of need for such information by practitioners. However, the loss of a number of major coastal bridges due to storm surge and wave loading during the last decade has not only created a need for better information on water levels and waves heights but wave crest lengths as well. The length of the bridge over which the design wave is acting is necessary for computing the horizontal and vertical forces (as well as the moments created by these forces) imparted to the bridge superstructure. Equations for predicting horizontal and vertical forces per unit wave crest length on bridge superstructures have been developed and are now in the AASHTO document "*Guide Specification for Bridges Vulnerable to Coastal Storms"*. With little or no information available on wave crest lengths for storm-generated waves in coastal waters, the assumption has been that the design wave crest lengths are at least as long as the bridge span length, which can range from 20 ft to over 200 ft. This assumption could be overly conservative at some locations and for longer span lengths. The objective of this study was to develop a methodology for including wave crest length effects on the surge/wave load predictions for bridge superstructures.

Wind waves generated by tropical storms and/or hurricanes are very complex with wave components ranging in heights, frequencies (wavelengths) and directions. This confused sea can, however, be characterized by a "directional wave spectra" which describes the energy in the waves that are propagating in the various directions with a range of frequencies. Computer wave models such as SWAN compute the directional wave spectra at each node in the mesh for each time step during the simulation.

A synthetic sea surface can be generated from a directional wave spectrum, such as those produced by wave models or obtained through field measurements, if it is assumed that the spectra is uniform over the area of interest and that the phasing of the waves is random. Figure 1-1 displays an example directional wave spectra produce by SWAN. Wave frequency is plotted on the horizontal axis and wave propagation direction on the vertical axis. The color in each rectangle indicates the amplitude of the waves with that frequency and propagation direction. The color scale is shown at the right of the plot. Each rectangle represents a linear wave with a specific frequency, amplitude and direction. The relative phases of these waves are, however, unknown. Since the procedure used to generate a sea surface from the directional wave spectra requires that the phases are known, the assumption is made that they are random. Due to this random phase assumption it is then necessary to generate numerous sea surfaces for the same directional wave spectra in order to achieve statistically meaningful results for obtaining such water surface properties as wave crest lengths.

The water surface elevation in a storm-generated sea varies continuously in both space and time. The lengths of the wave crests will depend on the criteria used in their definition. If a horizontal plane is placed above the mean sea surface, the surface above the plane can be analyzed for wave crest lengths, i.e., the lengths of the continuously connected surfaces above the plane. These lengths will obviously depend on the elevation of the plane above the mean water level, the threshold elevation. Attempts to establish a

procedure for arriving at a meaningful threshold value were not successful. The arbitrariness of such a selection led to the development a different approach, which was successful. This approach eliminated the need to define a threshold value and in addition accounts for the crest height variation along the structure for waves approaching normal to the structure.

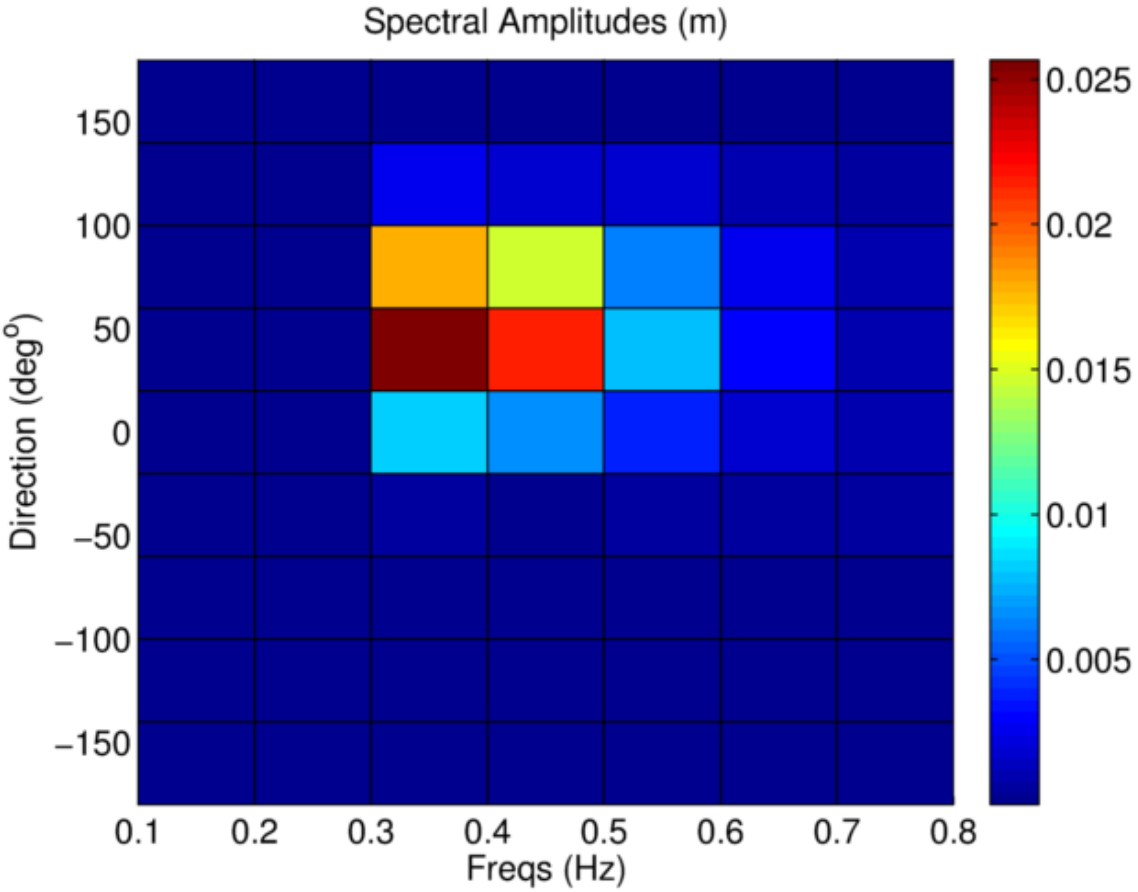

Figure 1-1 Example directional wave spectra showing spectral components and wave amplitudes color coded according to the scale on the right.

The format of this report is as follows. Chapter 1 is a brief overview of the work performed. Chapter 2 defines and explains wave spectra and its associated parameters. Chapter 3 summarizes the literature on sea surface simulations and measurements as well as the search performed for measured data. Chapter 4 gives an overview of available wave spectra produced by SWAN simulations at North Carolina bridge sites. These data were used in the development and testing of the methods for accounting for wave crest length on wave forces on bridge superstructures. Parametric wave spectra, which can be created without running wave models, were also used in this study. These parametric spectra, namely JONSWAP and TMA are introduced in Chapter 5. The details of sea surface simulations and analyses of wave crest lengths are described in Chapter 6. The effect of wave nonlinearity on wave crest lengths is also discussed in Chapter 6. Chapter 7 quantifies the effect of wave non-linearity and phase correlations based on measured

sea surface data. The surge/wave vertical force predictive equations for horizontal structures such as bridge superstructures indicate a linear dependence on wave height. This fact was utilized in the development of the new methodology explained in Chapter 8. Also in Chapter 8 is the application of the new methodology to a wide range of SWAN and JONSWAP wave spectra. These results were then used to develop empirical equations that can be used to apply the new methodology to cases where design wave spectra are not available. Procedures for applying the empirical equations for different levels of available met/ocean information are described in Chapter 9. In Chapter 10 the methodology is applied to the I-10 Bridges over Escambia Bay, which were severely damaged during Hurricane Ivan in 2004. The last chapter summarizes the findings of this study and discusses further research topics.

2.0 Wave Spectra and Wave Parameters

Prior to discussing three-dimensional real sea surfaces and associated wave spectra, a brief description of linear water waves is presented. Figure 2-1 is a definition sketch showing some of the properties of linear, monochromatic water waves. The linear wave has two dimensions, i.e. does not vary in the third dimension and has infinite wave crest length.

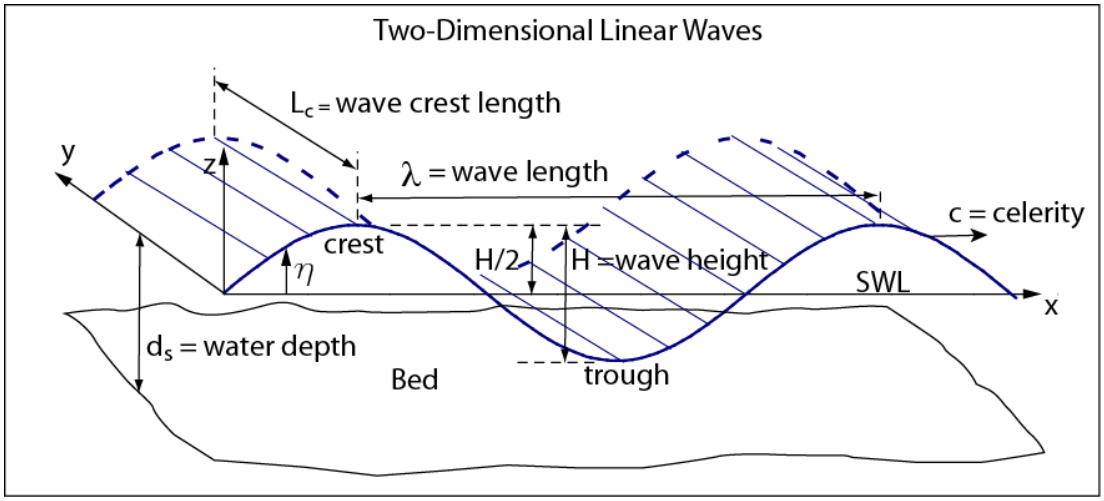

Figure 2-1 Definition sketch for linear waves.

Wave period T, wave length λ and water depth d_s are related with the dispersion equation. Various forms and approximations of this relationship are given in Table 2-1.

Table 2-1 Equations for wave height and wave length

	Shallow Water	**Intermediate**	**Deep Water**
	$d_s/\lambda < 1/20$,	$0.05 < d_s/\lambda < 1/2$	$d_s/\lambda > 1/2$
	$d_s/(gT^2) < 0.0025$	$0.0025 < d_s/(gT^2) < 0.08$	$d_s/(gT^2) > 0.08$
Wave Length	$\lambda = T\sqrt{g\,d_s}$	$\lambda = \frac{gT^2}{2\pi} tanh\left(\frac{2\pi d_s}{L}\right)$	$\lambda = \frac{gT^2}{2\pi}$
Wave Period	$T = \frac{\lambda}{\sqrt{g\,d_s}}$	$T = \sqrt{\frac{2\pi\lambda}{g \tanh(2\pi d_s/\lambda)}}$	$T = \sqrt{\frac{2\pi\lambda}{g}}$

Energy per unit surface area = $E = \frac{1}{2}\rho g a^2 = \frac{1}{8}\rho g H^2$

Energy per unit wave crest width = $E_T = \frac{1}{2}\rho g a^2 \lambda = \frac{1}{8}\rho g H^2 \lambda$

While monochromatic waves can be fully described by a period and a height, random waves are described by wave spectra, which is a surface showing the wave energy at different frequency, f and directions, θ. The two dimensional wave spectrum is represented by $S(f,\theta)$. Directional spectrum $D(\theta)$, frequency spectrum $E(f)$, and significant wave height are found by integrating $S(f,\theta)$ over the range of the appropriate variable (f or θ)

$$\begin{aligned} E(f) &= \int_0^{2\pi} S(f,\theta)\,d\theta \\ D(\theta) &= \int_0^{\infty} S(f,\theta)\,df \\ m_0 &= \int_0^{\infty} E(f)\,df \\ H_s &= 4m_0 \end{aligned} \tag{1}$$

where m_0 is the area under the frequency spectrum. Note that sometimes significant wave height is defined as the average of the highest one third waves, $H_{1/3}$. These two definitions are almost equal for deep water, but might differ under some conditions. The spectral definition is used in this study. An example two dimensional wave spectrum and its associated one directional counterparts are shown in Figure 2-2. Peak frequency, f_p and peak direction are shown with red dashed lines. Moments of the frequency spectrum are defined as

$$m_i = \int_0^{\infty} f^i E(f)\,df \tag{2}$$

The zeroth moment m_0 is the area under the curve $S(f)$ and the first moment m_1 is the mean frequency f_m. Other related wave parameters are

$$\begin{aligned} T_m &= 1/f_m \\ T_p &= 1/f_p \\ \lambda_m &= \text{Wave length associated with } T_m \\ \lambda_p &= \text{Wave length associated with } T_p \end{aligned} \tag{3}$$

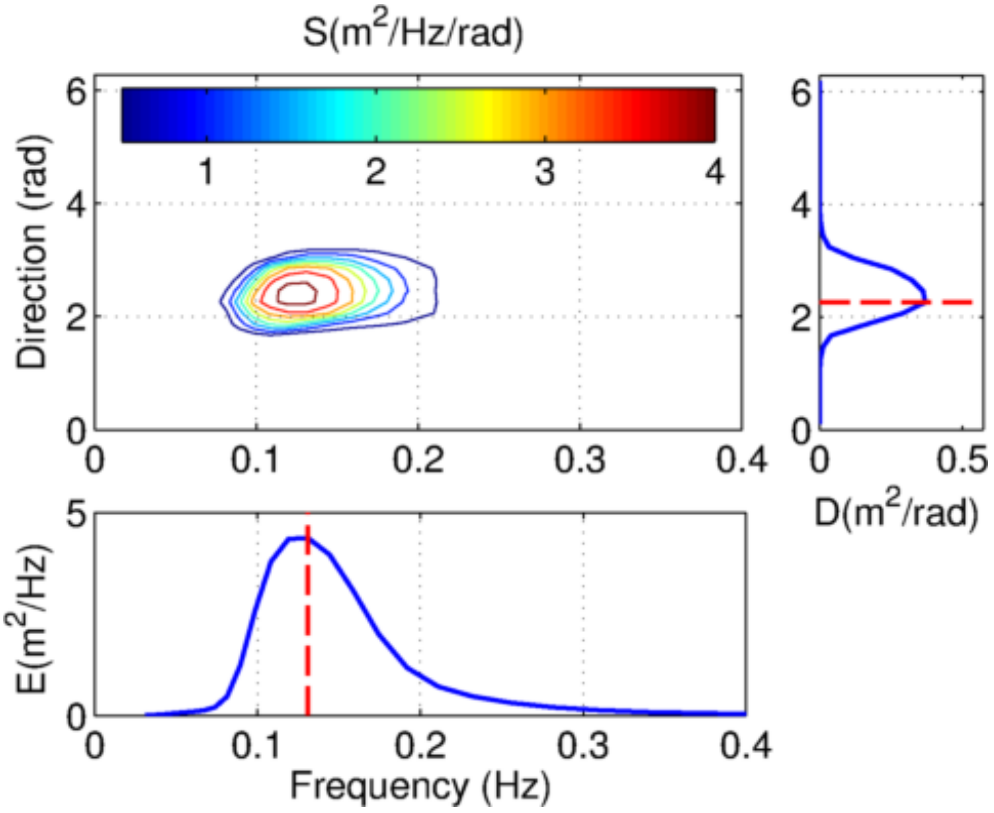

Figure 2-2 Example 2D and 1D spectrum

The spectral bandwidth parameter is defined as:

$$\varepsilon = \sqrt{1 - \frac{m_2^2}{m_0 m_4}}\ , \tag{4}$$

where m_i is the *i*th spectral moment defined in Equation (2).

The frequency spreading parameter is defined as

$$F_{spr} = \frac{\left| \int_0^{\infty} E(\omega) e^{i\omega T} d\omega \right|}{m_0}, \tag{5}$$

The directional spreading parameter (in degrees) is defined as

$$D_{spr}{}^2 = \left(\frac{180}{\pi} \right)^2 \int_0^{2\pi} 2 \sin\left(\frac{\theta - \bar{\theta}}{2} \right) D(\theta) d\theta\ , \tag{6}$$

Small directional spreading shows that all the waves are coming from a narrow band of directions as seen in a swell. Large directional spreading is more likely to be seen in a wind sea.

The peakedness parameter Q_p is defined as:

$$Q_p = 2\frac{\iint f S^2(f,\theta)\,df\,d\theta}{\left(\iint S(f,\theta)\,df\,d\theta\right)^2}\ , \tag{7}$$

A large peakedness parameter shows that the most wave energy is in a small frequency band and the sea state is more organized.

3.0 Literature Review and Data Search

Wave crest lengths have attracted much less attention compared to other properties of waves due to the limited need for this parameter and also the large resource requirements for their measurement and/or prediction. Longuet-Higgins analyzed wave crest statistics both for linear (Longuet-Higgins 1957) and non-linear cases (Longuet-Higgins 1963). He defined a long-crestedness parameter. However, he did not analyze wave crest length. Tucker et al. (1984) pointed out that when simulating time series from wave spectra, spectral amplitudes need to be treated as random variables with an expected value equal to the spectral amplitude. Otherwise, the variance of different time series realizations are underpredicted, which results in an underprediction of extreme events. Elgar et al. (1985) showed that if there are more than 1000 spectral components, underprediction does not occur, even without random amplitudes. Goda (1994a) simulated wave surfaces from parametric wave spectra for different water depths and developed empirical relationships for mean crest lengths as a function of equivalent spreading parameters. The spreading parameter is a measure of the directional spreading of the waves. He showed that water depth does not influence wave crest length normalized by wave length when linear theory is used in the development of the water surface.

Monaldo (2000) measured wave crest lengths during Hurricane Josephine 1984 and Hurricane Bonnie 1998 using Synthetic Aperture Radar (SAR) images. He also compared measured wave crest lengths to simulated wave crest lengths and found the simulations to underpredict the measurements in some cases by varying amounts. Long wave dispersion, creating correlations between phases, and non-linear wave-wave interactions were offered as possible reasons for the difference. This is the only paper in the literature that calculates crest length statistics from sea surface measurements. Forristall (2000) compared wave crest statistics from measurements with those from non-linear sea surface simulations. He showed that nonlinear effects increased wave crest area as much as 100%. The non-linear analysis was based on the work by Longuet-Higgins (1963) for deep water, which was expanded to intermediate water depths by Sharma and Dean (1979). Similarly Romero and Melville (2011) showed that nonlinearity effects can have a significant impact on total wave crest lengths per unit area. Scott et al. (2005) investigated total crest lengths per unit area for steep waves. However, it should be noted that the wave crest parameters investigated in these three studies are different from the absolute crest lengths that are of interest in this research project. That is, individual wave crest lengths cannot be extracted from wave crest lengths per unit surface area. Other studies that collected sea surface images in deep water without analyzing the data for wave crest lengths include Banner et al. (1999), Hwang et al. (2000) and Reineman et al. (2009).

Information and Data Search

The following people and institutions were identified and contacted regarding their having measured sea surface data.

Table 3-1 List of people and institutions contacted for sea surface data

Institution	**Person**	**Status**
NASA Jet Propulsion Laboratory	Yoseph Bar-Cohen	Contacted. Forwarded to Phillip Callahan
NASA Jet Propulsion Laboratory	Phillip Callahan	Expertise in satellite measurements. Satellite data is not ideal. Will not contact at this stage.
Exxon-Mobile	Long, Louis G	Contacted. No data available
Chevron	Justin Marin	Contacted. No Response.
Remote Sensing Division, Naval Research Laboratory	Paul A. Hwang	Contacted. Forwarded to Ken Melville
Physical Oceanography Research Division of Scripps	Ken Melville	Contacted. Deep water data available.
NOAA Storm Surge Group	Jamie Rhome	Contacted. Forwarded to Edward Walsh
NOAA Physical Sciences Division	Edward Joseph Walsh	Contacted. Deep water data available.

Edward Joseph Walsh with NOAA and Ken Melville at Scripps Institute of Oceanography both have measured sea surface data. Dr. Melville emailed copies of several of his papers on this subject. Both datasets are, however, for offshore, deep water conditions where the wave parameters are different.
No sea surface data for shallow, closed or partially closed waters were located in this search.

4.0 Spectra from SWAN Simulations

As a part of a separate OEA study, wind, atmospheric pressure, water surface elevation, waves and depth-averaged currents were simulated for 186 hurricanes throughout North Carolina coastal waters using a coupled ADCIRC-SWAN model. Although SWAN is a spectral wave model, wave spectra are not usually saved due to computer storage space and increased computation time considerations. However, OEA has saved the wave spectra for each simulation time step for 186 storms at 172 locations. This resulted in a dataset of more than 15 million directional wave spectra for this project. Figure 2-1 shows the locations of the saved directional wave spectra in the coastal and nearshore waters of North Carolina.

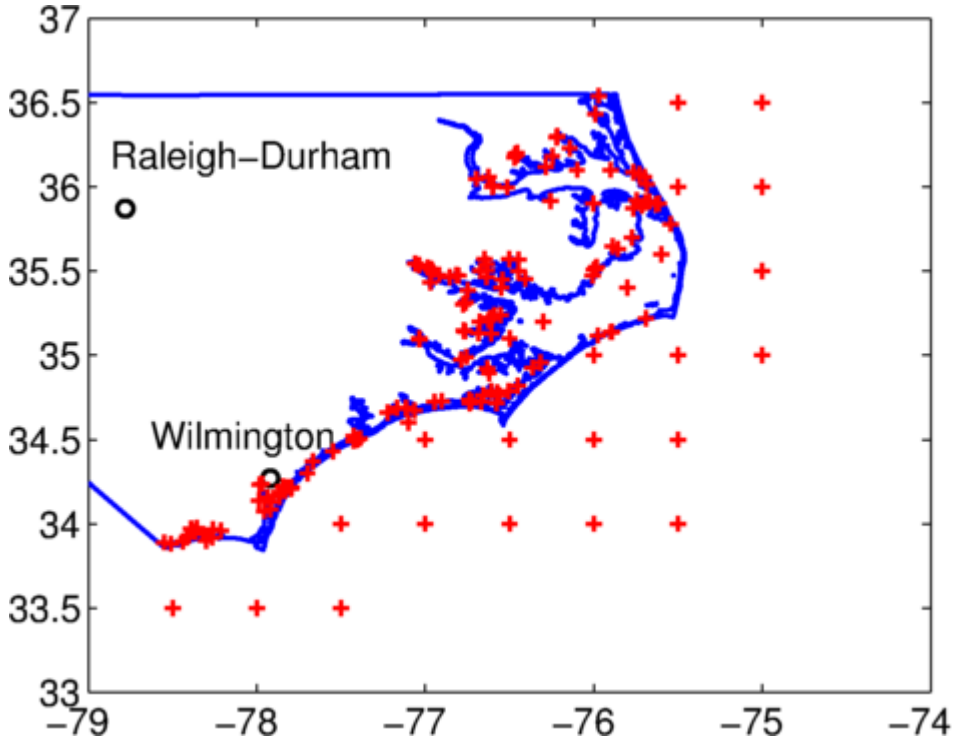

Figure 4-1 Locations of wave spectra collected from SWAN simulations

For each hurricane the spectra with the highest energy at each site was identified and extracted. The highest energy cases were chosen since it is those conditions that are used in the computation of design surge/wave loads on the bridge superstructures. The following parameters were computed for approximately 5,060 wave spectra.

- Significant wave height, H_s
- Mean wave period, T_m
- Peak wave period, T_p
- Peak wave direction, θ_p
- Directional spreading parameter, D_{spr}
- Frequency spreading parameter, F_{spr}

- Spectral peakedness parameter, Q_p
- Spectral bandwidth parameter, ε

Removing waves with H_s smaller than 0.5 m, reduced the number of spectrum from 5,060 to 2,690. Figure 4-2 shows the distribution of spectral parameters F_{spr}, ε, Q_p, and D_{spr} for the SWAN simulations. The first three are functions of the shape of the frequency spectrum and are correlated to varying degrees. D_{spr} is a function of the directional distribution and is independent of the other parameters. The distribution of significant wave height H_s, mean period T_m, peak period T_p, and peak wave length l_p are presented in Figure 4-3. Most of the data has small wave heights, periods and wave lengths since they are in shallow water. The correlations among parameters are generally high as expected, since the last three parameters are directly related. Figure 4-4 shows the distribution of parameters from the two previous plots. There is no obvious correlation between the spreading parameters and the wave properties. The variation of the spreading parameters is large for smaller waves, but this is probably due to the fact that there are significantly more small waves.

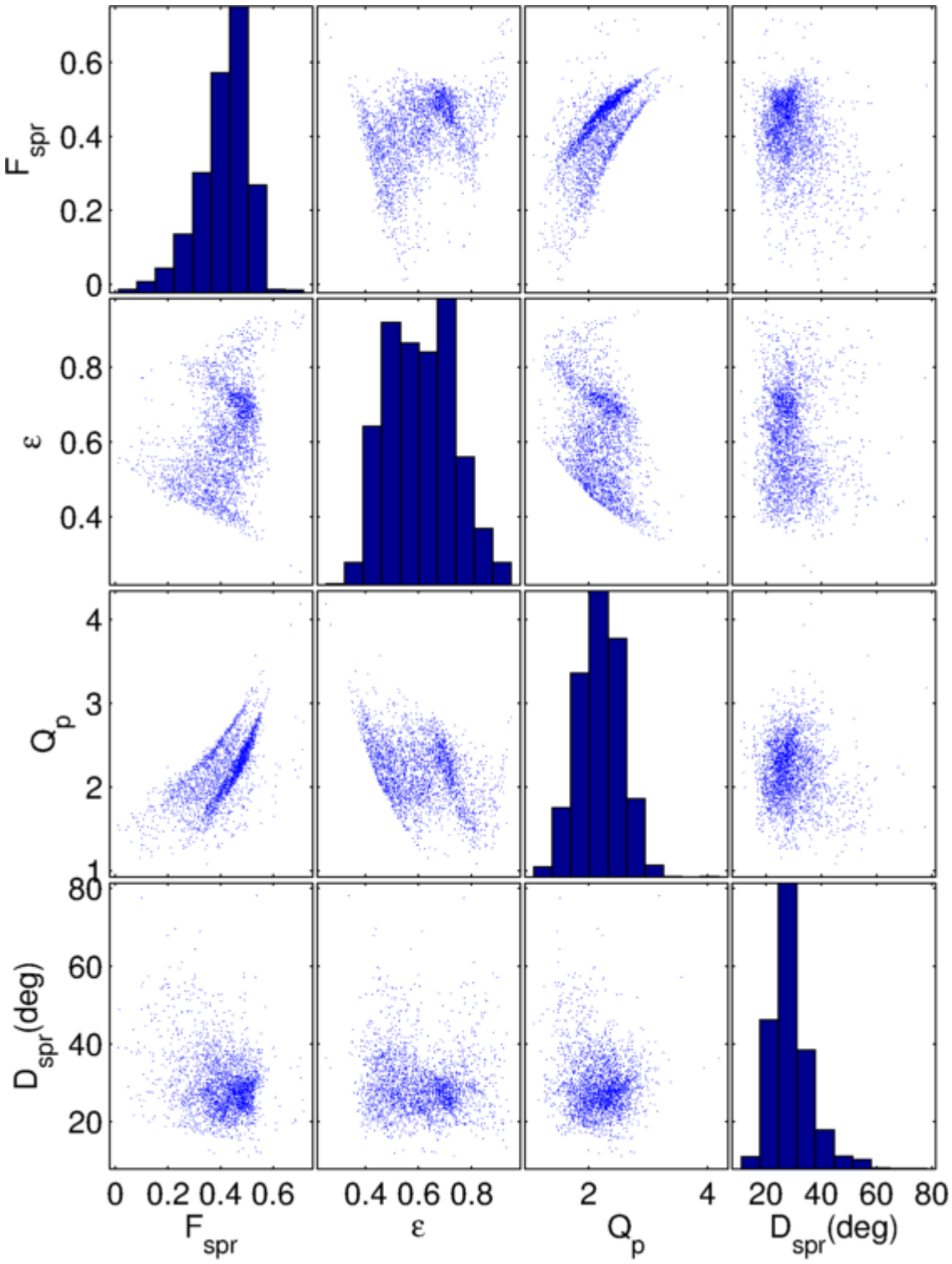

Figure 4-2 Distribution of spectral parameters F_{spr}, ε, Q_p, and D_{spr} for SWAN simulations.

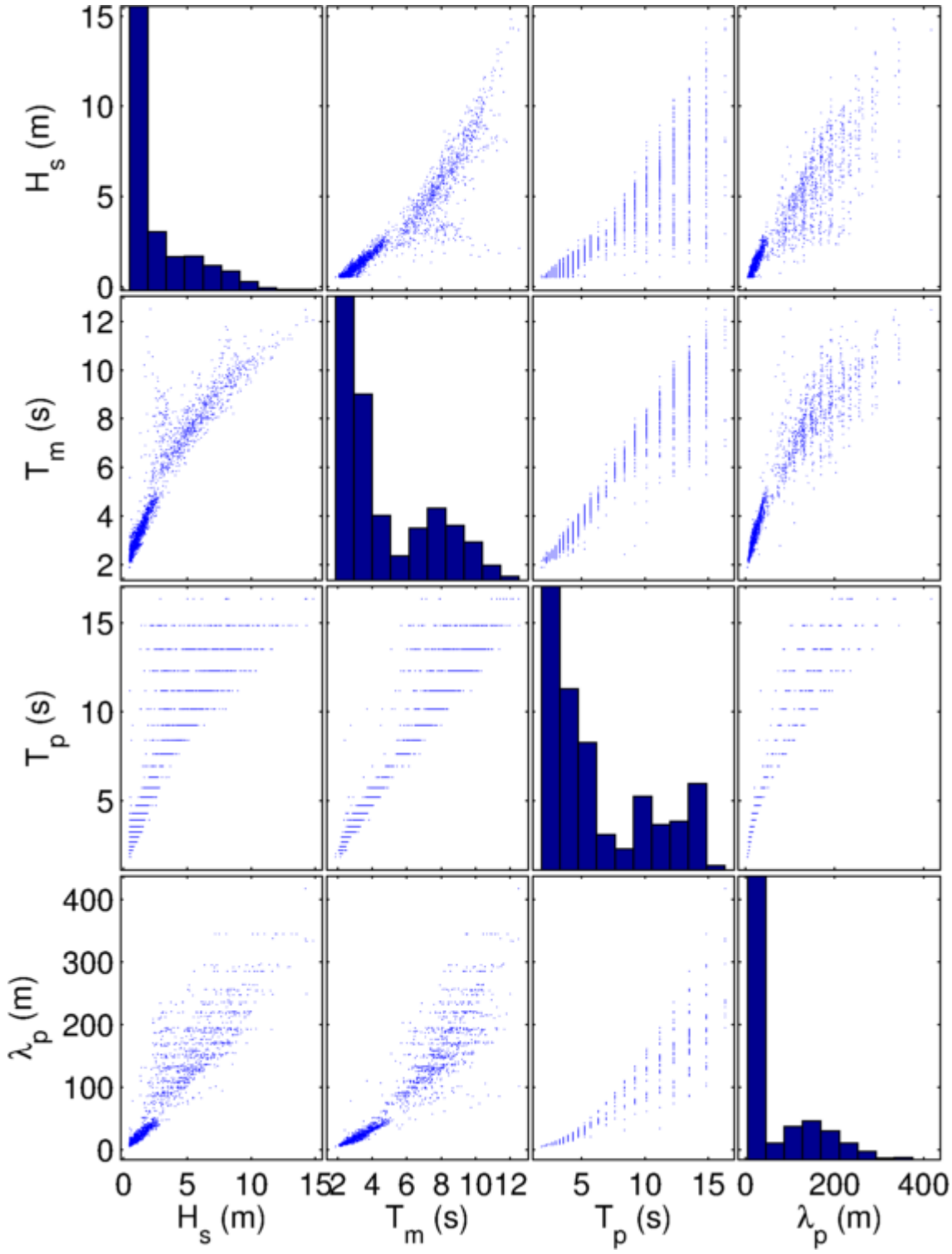

Figure 4-3 Distribution of wave parameters H_s, T_m, T_p and λ_p for SWAN simulations.

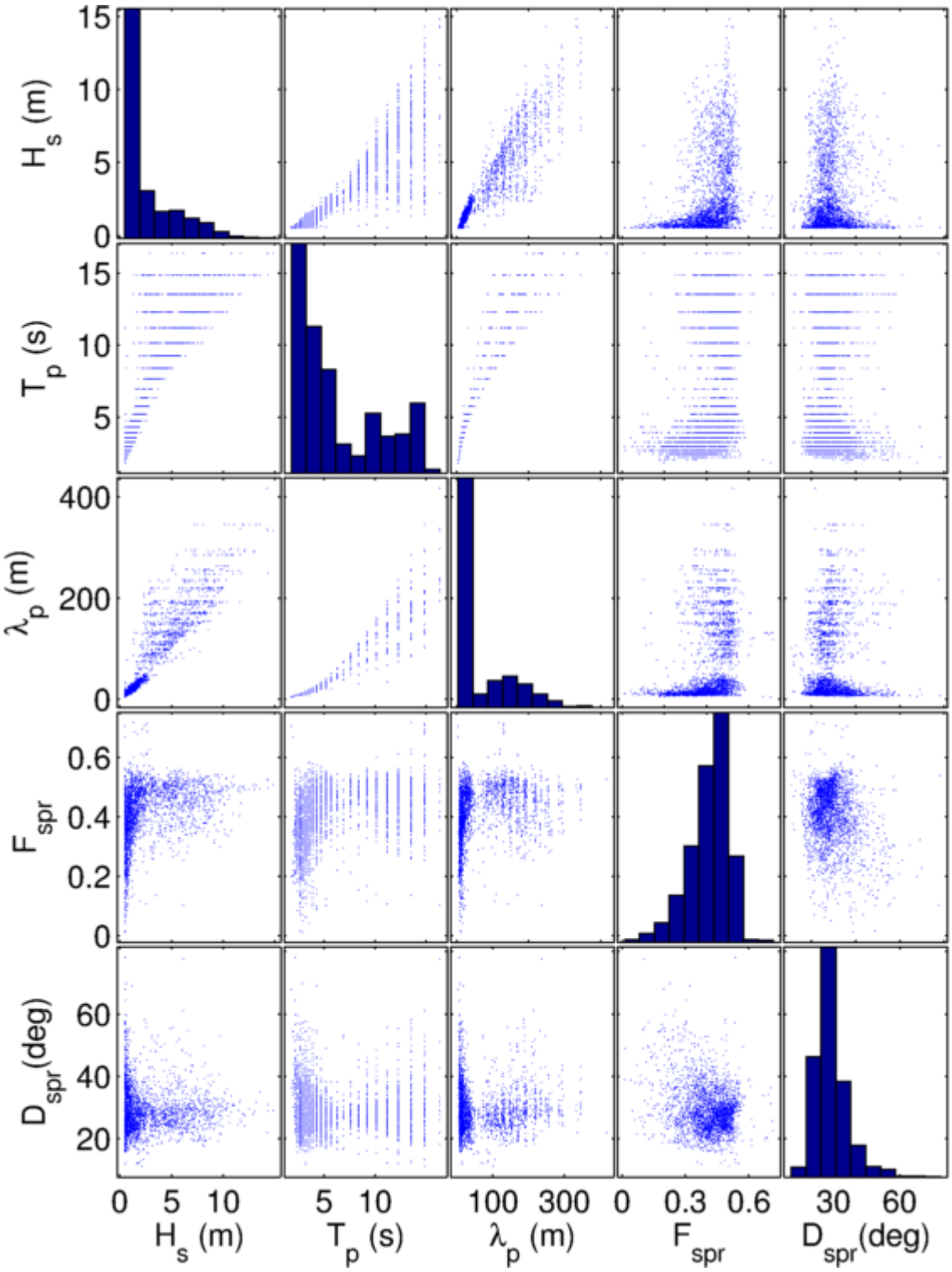

Figure 4-4 Distribution of parameters H_s, T_m, $L_{p,}$ $F_{spr,}$ and D_{spr} for SWAN simulations.

5.0 Parametric Spectra

For locations where a Level III storm surge and wave analysis has been performed, directional wave spectra exist at each time step throughout the study area for all of the hindcasted storms. For these situations, the sea surface near the peaks of these storms can be simulated for each hindcasted storm as previously discussed. While this type of information is very useful for aspects of this project, it does not allow for the determination of the dependency of wave crest lengths on the various spectral parameters. For this type of analysis, it is more appropriate to analyze sea surfaces simulated using parametric spectra. Parametric spectra have been developed for different conditions based on measured wave data.

One type of wave spectrum thatwas used in this study is JONSWAP. It was developed for fetch limited conditions in deep water. The JONSWAP spectrum was originally formulated in terms of fetch length and wind speed. The form that was cast in terms of wave properties by Goda (1994a) was used in this project:

$$
\begin{aligned}
&\mathrm{E}(f) = \beta_j \mathrm{H_s^2 T_p^{-4}} f^{-5} exp\left(\left[-1.25 \left(\mathrm{T_p} f \right)^{-4} \right] \gamma^{exp\left(-\frac{(\mathrm{T_p} f - 1)^2}{\sigma^2} \right)} \right) \\
&\beta_j = \frac{0.0624\left[1.094 - 0.01915 \ln(\gamma)\right]}{0.230 + 0.336\gamma - 0.185(1+\gamma)^{-1}} \\
&\sigma = \begin{cases} 0.07, & f \le f_p \\ 0.09, & f > f_p \end{cases}
\end{aligned}
\tag{8}
$$

where γ is the peak shape parameter, G is Mitsuyasu Directional Spreading which has a dependence on frequency.

$$
\begin{aligned}
&\mathrm{G}(f,\theta) = \mathrm{G}_0 cos^{2\mathrm{sp}}\left(\frac{\theta}{2}\right) \\
&\mathrm{G}_0 = \left[\int_{\theta_{\min}}^{\theta_{\max}} cos^{2sp}\left(\frac{\theta}{2}\right) d\theta \right]^{-1} \\
&\mathrm{sp} = \begin{cases} \left(f / f_p \right)^5 \mathrm{sp}_{\max}, & f \le f_p n / 2 \\ \left(f / f_p \right)^{-2.5} \mathrm{sp}_{\max}, & f > f_p \end{cases}
\end{aligned}
\tag{9}
$$

sp_{max} is the Mitsuyasu Directional Spreading Parameter with a typical range of 10 (wind waves) to 75 (swell). Note that sp_{max} is different than directional spreading parameter D_{spr}

defined earlier. D_{spr} is a measure of directional spreading that can be calculated for any spectrum, while sp_{max} is a measure of directional spreading for a specific parametric directional spreading function namely G, Mitsuyasu Directional Spreading and it is not calculated, but specified.

The four free parameters of this spectrum are the wave height (H_s), wave period (T_p), peak shape parameter (γ) and the Mitsuyasu Directional Spreading Parameter (sp_{max}). An example spectrum is shown in Figure 5-1. Wave height is just a constant that changes the magnitude of the spectra without changing its shape.

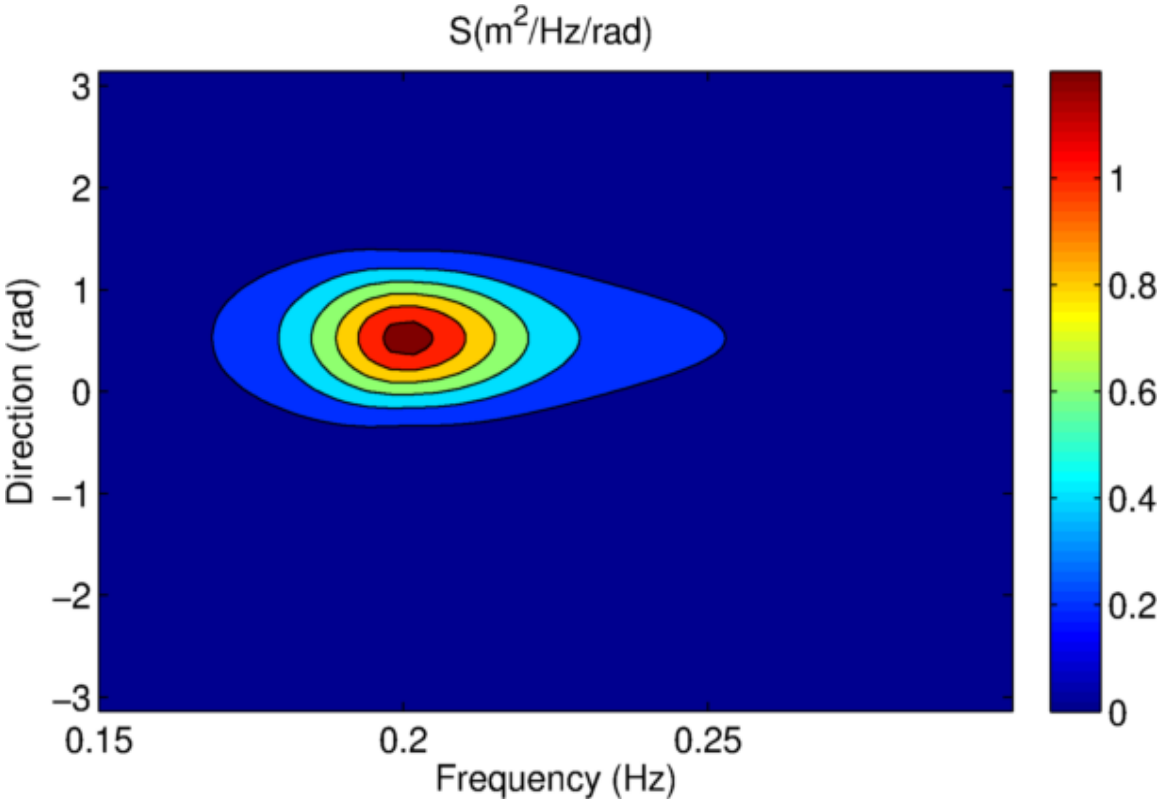

Figure 5-1 Example JONSWAP spectra with Mitsuyasu-type directional spreading. (H_s=1 m, γ=3.3, T_p=5 sec, sp_{max}=10, Peak direction=π/6)

Another type of spectrum used in this study is the TMA spectrum. It is the JONSWAP spectrum scaled to finite water depths:

$$
\begin{aligned}
&\mathrm{E}_{\mathrm{TMA}}\left(f,\mathrm{d_s}\right)=\phi\left(f,\mathrm{d_s}\right)\mathrm{E}_{\mathrm{JONSWAP}}\left(f\right)\\
&\phi\left(2\pi f,\mathrm{d_s}\right)=\frac{\mathrm{k}\left(\omega,\mathrm{d_s}\right)^{-3}\dfrac{\partial \mathrm{k}\left(\omega,\mathrm{d_s}\right)}{\partial\omega}}{\mathrm{k}\left(\omega,\infty\right)^{-3}\dfrac{\partial \mathrm{k}\left(\omega,\infty\right)}{\partial\omega}}\\
&=\frac{\mathrm{k}\left(\omega,\infty\right)^{3}}{\mathrm{k}\left(\omega,\mathrm{d_s}\right)^{3}\left(tanh\left(\mathrm{k}\left(\omega,\mathrm{d_s}\right)\mathrm{d_s}\right)+\dfrac{\mathrm{k}\left(\omega,\mathrm{d_s}\right)\mathrm{d_s}}{cosh(\mathrm{k}\left(\omega,\mathrm{d_s}\right)\mathrm{d_s})^{2}}\right)}\\
&\omega=2\pi f\\
&\mathrm{k}=\frac{2\pi}{\lambda\left(\omega,\mathrm{d_s}\right)}
\end{aligned}
\tag{10}
$$

where ω is the radial frequency and k is the wave number. The JONSWAP spectrum in Figure 5-1 is scaled to 7 m water depth and the resulting TMA spectrum is shown in Figure 5-2. The total energy decreases and the significant wave height drops to 0.78 m. Some of the energy shifts to higher frequencies, the mean frequency decreases but the peak frequency does not change.

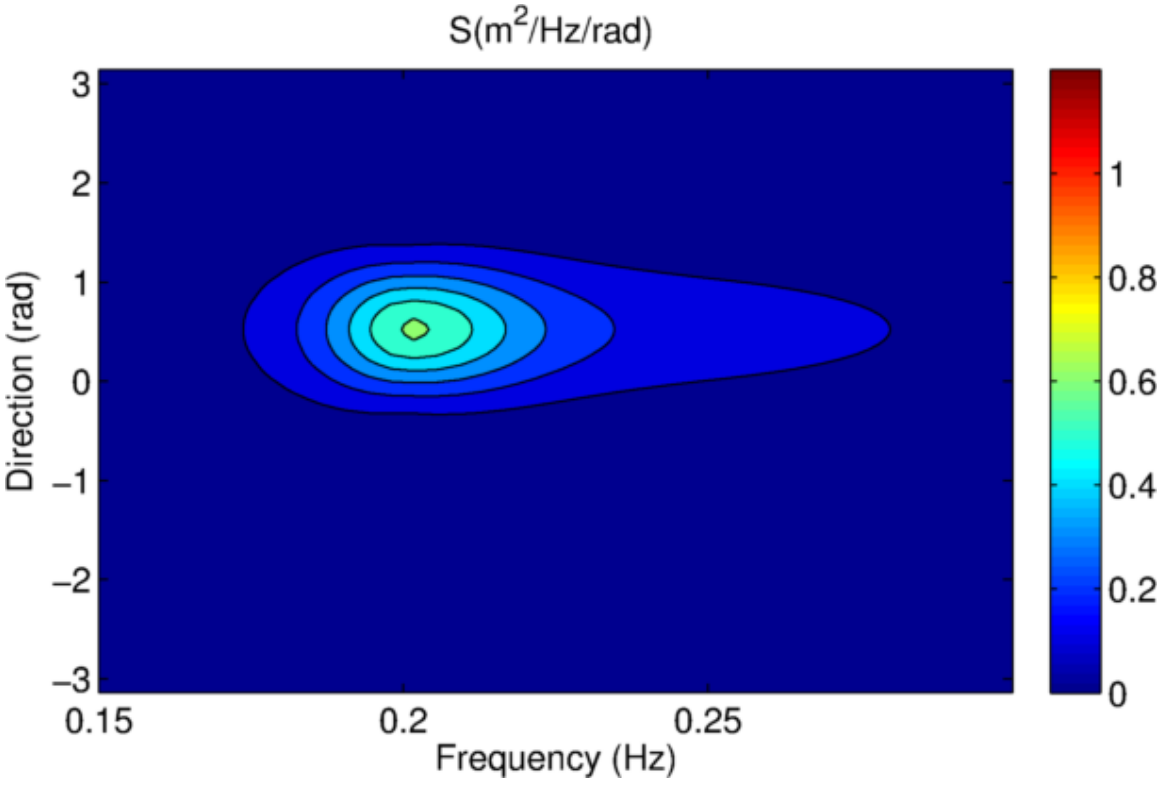

Figure 5-2 Example TMA spectra with Mitsuyasu-type directional spreading. (depth= 7 m, H_s=0.78 m, γ=3.3, T_p=5 sec, sp_{max}=10, Peak direction=π/6)

6.0 Sea Surface Simulation from Wave Spectra

The sea surface elevation η, which varies in time and space, can be simulated by summing a finite number of the Fourier components. The resulting sea surface is has a Gaussian distribution.

$$\eta\left(\vec{x},t\right)=\sum_{m=1}^{M}\sum_{n=1}^{N}a_{m,n}cos\left(\overrightarrow{k_{m,n}}\vec{x}-\omega_n t+\varepsilon_{m,n}\right) \tag{11}$$

$$a_{m,n}=\sqrt{S(k_{m,n},\omega_n)\Delta k\Delta\omega} \tag{12}$$

where m and n are the indices for different wave frequencies and directions respectively, $a_{m,n}$ are the component wave amplitudes and ε is a random phase which has a uniform distribution. However, there is disagreement in the literature about the form of the amplitudes. Tucker et al.(1984) recommended using a Rayleigh distribution with an expected value equal to the value given in Equation(12). Goda in his 1994 publication (1994a) used a deterministic amplitude. Later (1999) he used a χ^2 distribution with two degrees of freedom. Forristal (2000) argued that a χ^2 distribution is needed only for a one dimensional frequency spectrum and that the two dimensional directional spectrum creates the χ^2 distribution naturally. Monaldo (2000) used the χ^2 distribution for a two dimensional spectrum. Figure 6-1 shows the comparison of wave crest lengths calculated using the three different methods discussed. For low wave crest lengths all three are in agreement, as expected, however, they differ for the more extreme events (the right side of the plot). It should be noted that the curves span more than four orders of magnitude and the differences in these methods only become apparent for very rare events. The deterministic method has the least variance and the χ^2 distribution the largest. The more conservative χ^2 distribution was used with directional spectra in this study.

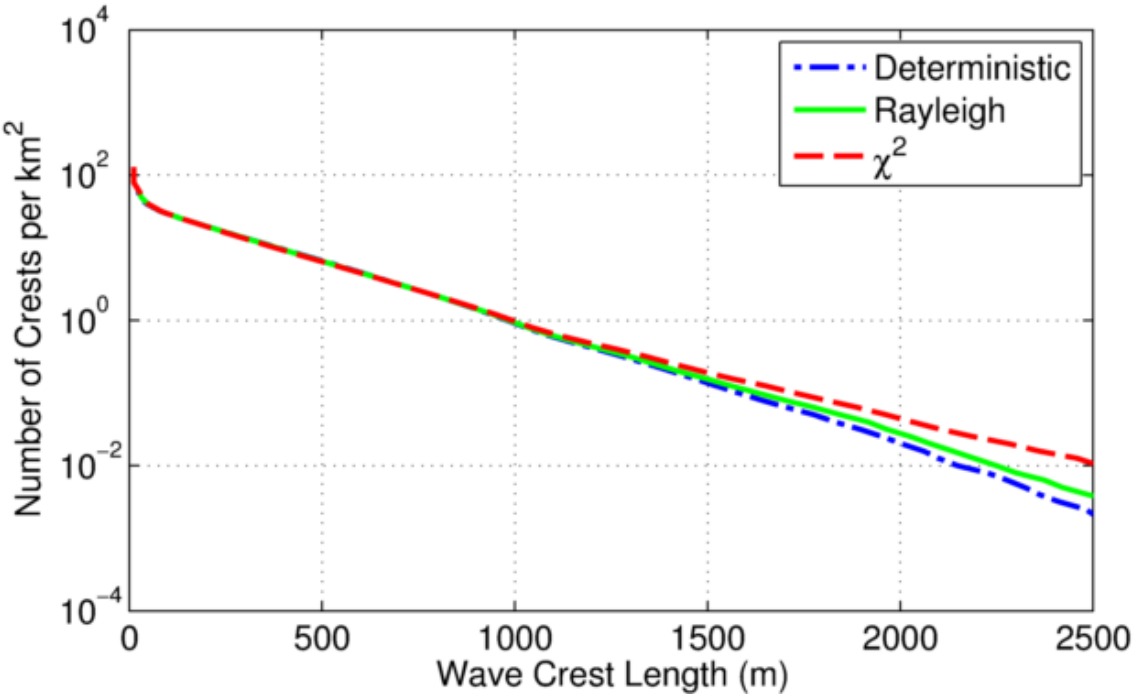

Figure 6-1 Crest length distributions computed using different methods of calculating wave component amplitudes.

6.1 Identification of Wave Crests

Some data processing is usually required for both simulated and measured sea surface images prior to identifying wave crest lengths. Images from measurements are generally preprocessed to remove noise and measurement artifacts. This typically involves applying filters in the frequency and spatial domains. Most of these steps are not necessary for simulated spectra, but should be used if the results from the two methods are to be compared.

An example of a simulated sea surface is shown in Figure 6-2. The significant wave height is 2 m, the period is 10 seconds, the sp_{max} is 10, and γ is 3.3. The wave crests are shown in red and the troughs in blue. Using a threshold value of $0.1H_s$ the image is converted into a binary image where the crest are shown in black (Figure 6-3). By calculating the connectivity of each pixel all of the crests are identified. To distinguish between the different crests each has a different color (Figure 6-4).

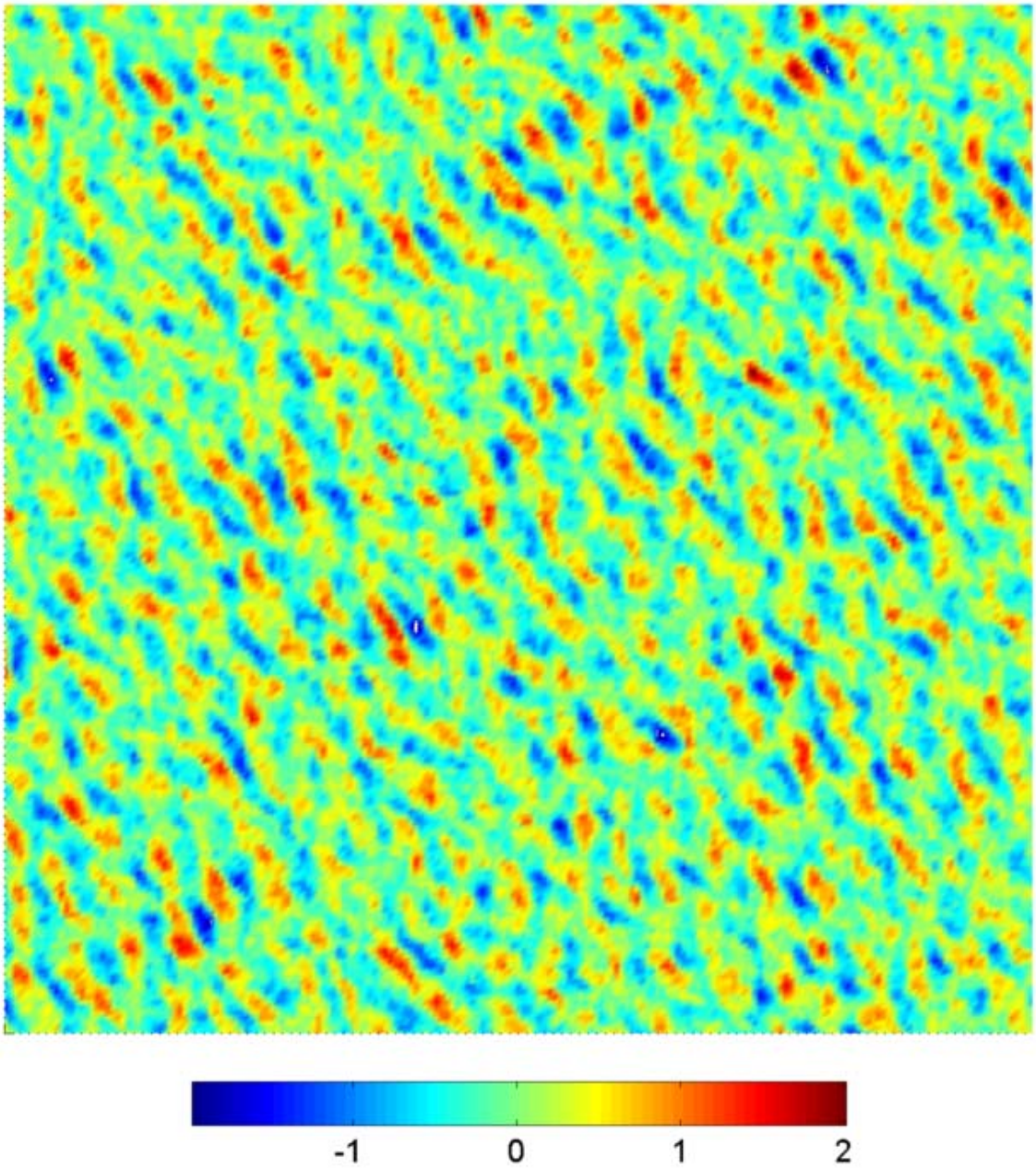

Figure 6-2 Color map of a simulated sea surface.

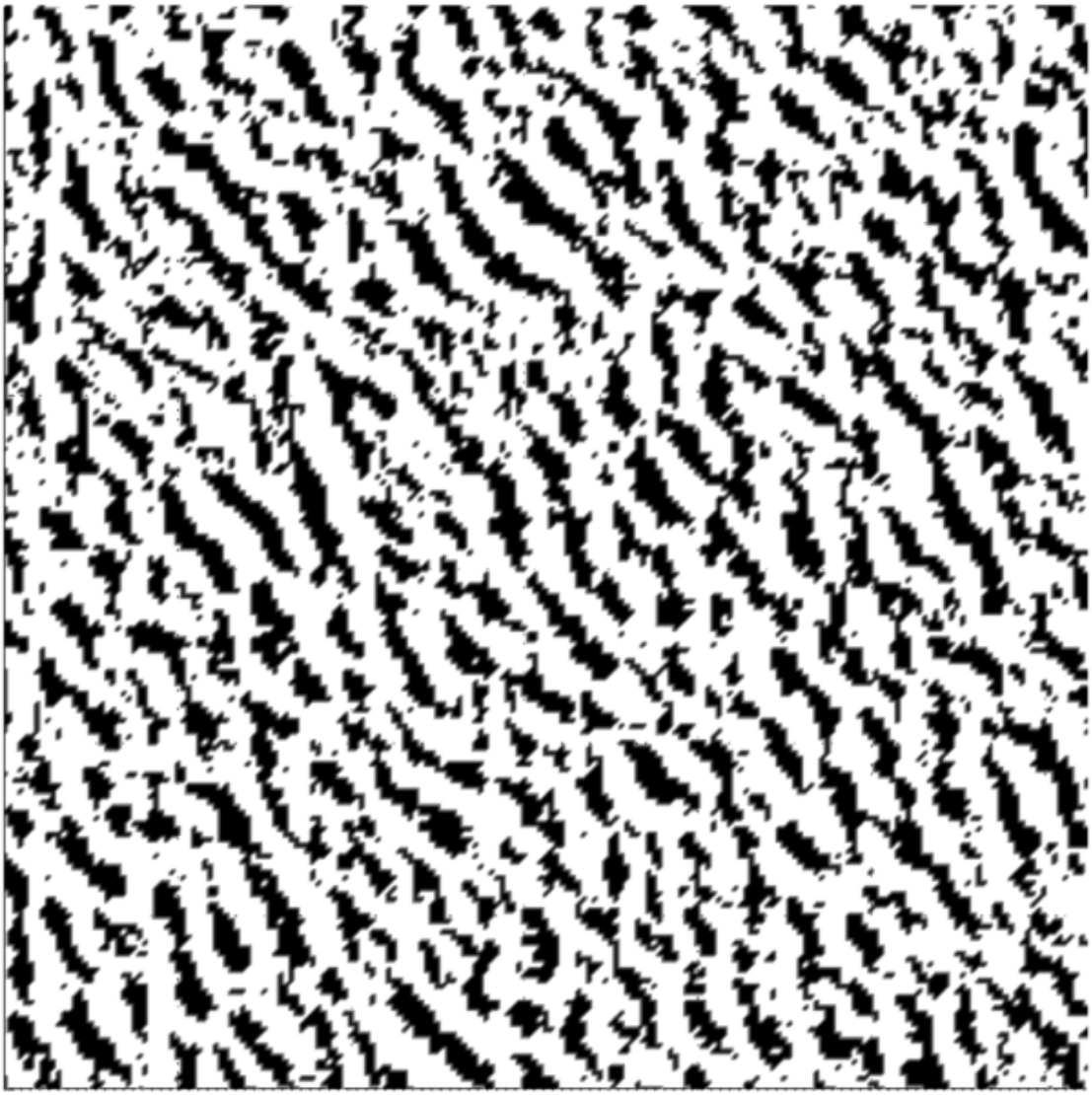

Figure 6-3 Sea surface image converted to binary image using a threshold value of 0.1 H_s.

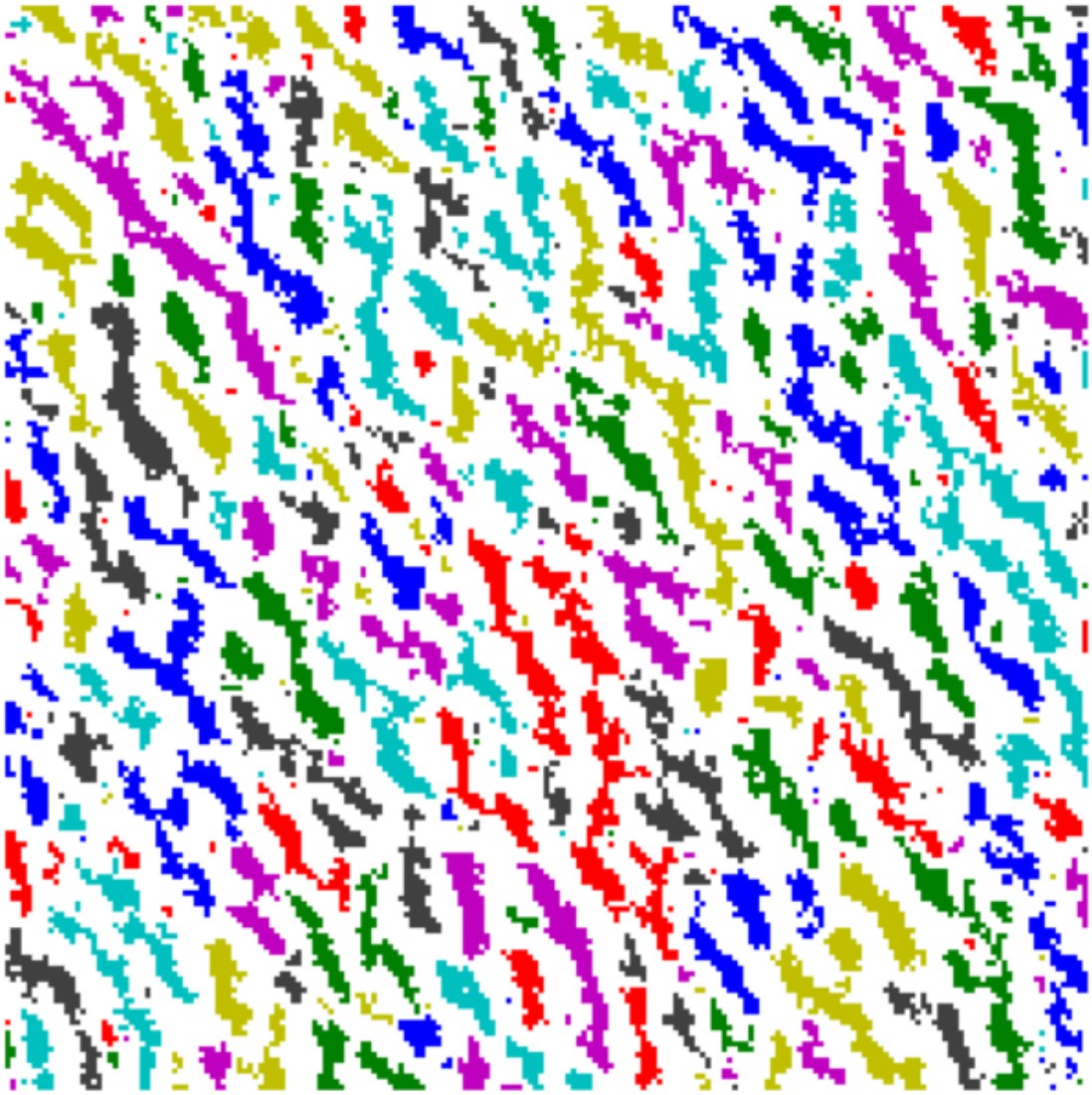

Figure 6-4 Individual wave crests identified from the threshold image (Figure 6-3).

When all the wave crests are identified an ellipse is fitted to each. The wave crest length, L_c is then assumed to be the length of the major axis of the ellipse. A distribution of wave crest lengths in the area can then be obtained. Figure 6-5 shows the distribution of wave crest lengths for this example. The horizontal axis is wave crest lengths and the vertical axis is the number of wave crest lengths per square km exceeding the length in the x-axis. The data for this plot comes from 2,500 repetitions of a simulation over an area 2000 m by 2000 m. Approximately 1.6 million wave crests were identified during the analysis. The number of wave crests decrease logarithmically with crest length except at the two extremes. The deviations at the extremes are due to the limitations of the simulation parameters. At the lower end of the curve the least the wave crest length can be is one pixel (10 m by 10 m for this simulation). The upper limit on the wave crest length is the diagonal distance of the simulation area which is $2000\sqrt{2} \approx 2828$. The crest lengths

longer than 2,500 m appear to be affected by this limitation as well. Only 1 out of 10,000 waves reach this value and can be ignored for the purposes of this study.

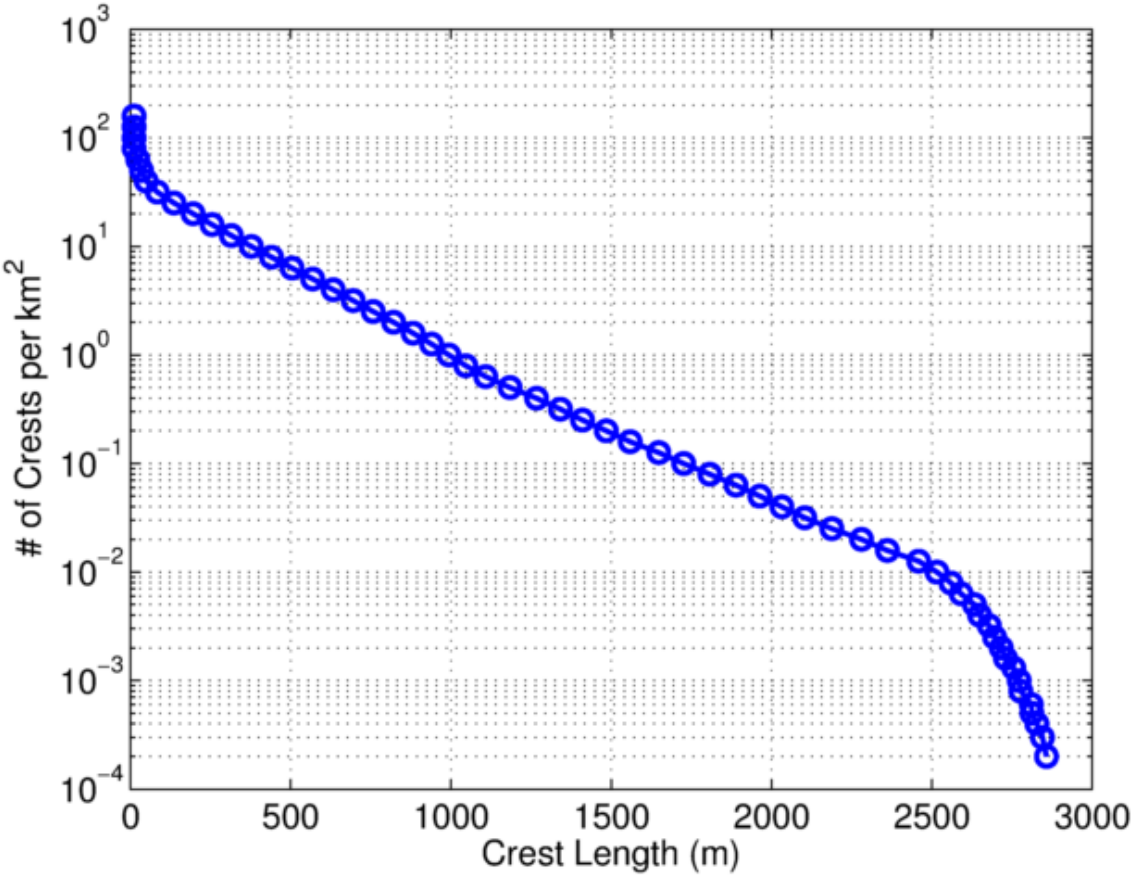

Figure 6-5 Distribution of wave crest lengths exceeding a given length.

Most of the waves are very small. Sixty eight percent of the waves have crest lengths one or two pixels long. The histogram in Figure 6-6 gives the distribution of small wave lengths. In terms of design conditions these waves are not relevant. They can be eliminated by using a minimum wave crest length or area threshold. For example Monaldo (2000) used 150 m^2 as a minimum area threshold. However, the statistical properties of the wave crest population such as mean, significant or rms (root mean squared) wave length will be a function of this arbitrary threshold.

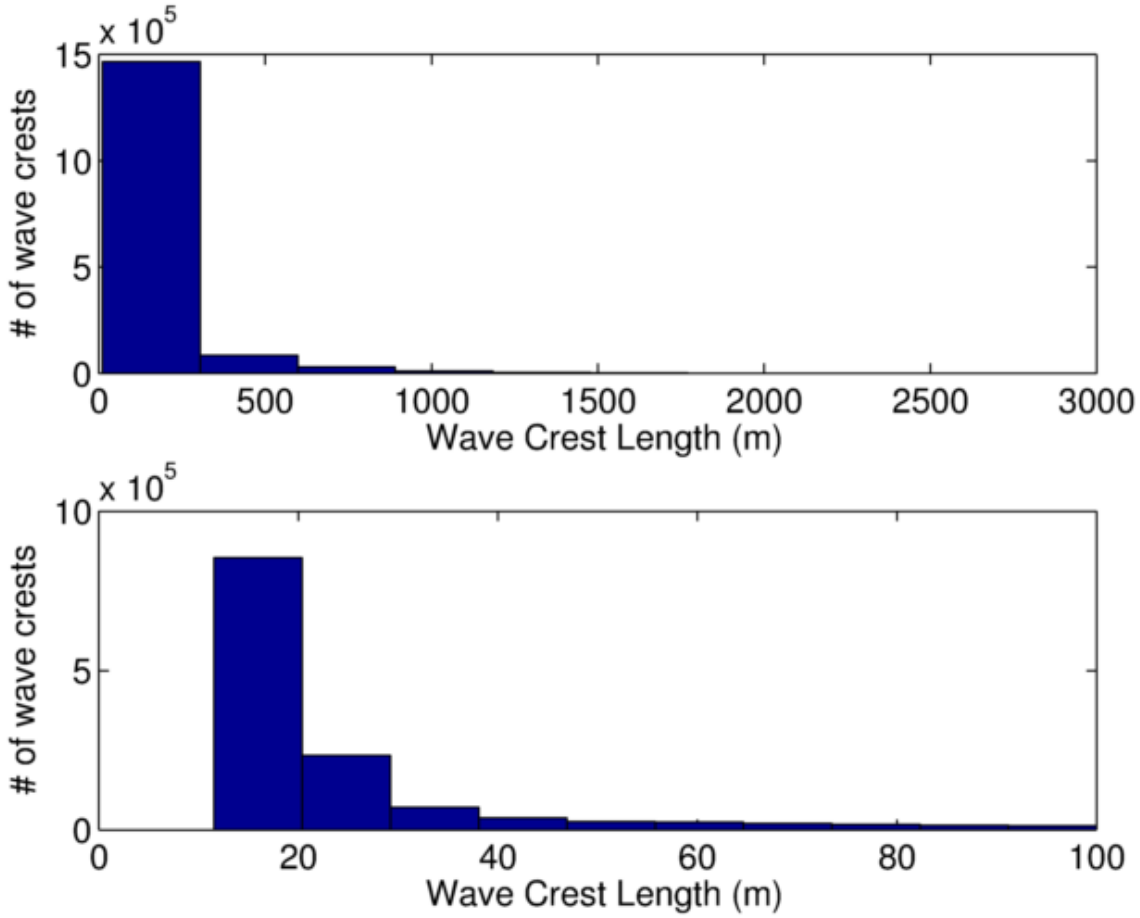

Figure 6-6 Distribution of the number of wave crest lengths per square kilometer exceeding the length on the horizontal axis for the example surface simulation. Top: Whole range of crest lengths. Bottom: Only waves with crest lengths smaller than 100 m.

6.2 Joint Distribution of Wave Crest Heights and Lengths

For all the wave crests identified, a wave crest height and length can be calculated. The highest elevation along the crest can be used to define the wave height. The rms elevation could also be used for the wave height definition. Figure 6-7 shows the joint distribution of relative maximum crest height (η_c/H_s) vs. relative crest length (L_c/λ_p). The numbers on the contour lines show the density of wave occurrence and are dependent on the total number of simulations. The relative values of those numbers are important and show that the vast majority of the waves have small wave heights and crest lengths. Figure 6-8 is a similar plot except rms wave heights are used. Note that the waves with the shortest crest lengths also have the least crest heights. The longest crests occur around 0.85 of the relative maximum crest height and 0.35 of the relative rms crest height. Goda (1994b) observed that the mean of the crest lengths do not change for waves with relative maximum crest heights of 0.75. This, however, was due to the limited number of simulations that he performed. Goda performed only 25 simulations whereas 2500 were performed in this study. Figure 6-9 shows the mean relative wave crest lengths as a function of relative wave crest height. The top parts of the curves are unreliable and they

do not follow the general trends of the curve because they represent only a few wave crests. The mean of the crest lengths reach a constant value only after a relative crest height equal to1.0. Rms crest heights peak at a relative crest height of 0.3 and then decrease, not converging to a constant value. Distribution of wave crests exceeding a given relative crest height are plotted in Figure 6-10. The difference between maximum and rms crest heights increases as crest height increases.

The problems with defining mean or significant crest length were discussed in the previous section. Using crests heights might be used for arriving at a working definition of crest lengths, but it introduces its own set of problems. 1.8 H_s is used as the design wave height in the AASHTO document "Guide *Specifications for Bridges Vulnerable to Coastal Storms"* (Modjeski and Masters et al. 2008). For linear simulations this corresponds to a relative crest height of 0.9. An rms crest height seems to be a more natural choice for use in wave force calculations, since wave forces are integrated over the span length. However, as seen in Figure 6-10 the rms relative wave height is not even close to 0.9 after 1.6 million waves. For a Rayleigh distribution 1.8 H_s corresponds to a 0.15% probability of exceedance. The distribution of the two dimensional rms crest height is obviously not the same as the distribution of wave heights at a single point. Relative maximum crest height does exceed 0.9, but it does not seem a good choice of wave height for wave force calculations. In conclusion, defining a wave crest length to be used in wave force calculations has various problems and requires many arbitrary decisions. Another approach that circumvents these problems was developed and is detailed in Chapter 7.0.

The results presented in this section are useful for interpreting the results of other studies specifically Monaldo (2000). As shown in Figure 6-9 the relative crest length of the waves with the highest rms crest height are about 2. Figure 6-11 shows the number of waves exceeding a given relative crest length. About 20 waves per km^2 exceed relative crest length of 2 and there are a total 80 waves per km^2 including all crest lengths. This shows that the relative crest length of the largest waves is exceeded by 25% of all waves. The crest lengths of design waves are not as rare as the wave heights; only 0.15% of the waves exceed those heights. This information is used in Chapter 8.0 to interpret the results from real sea surface measurements.

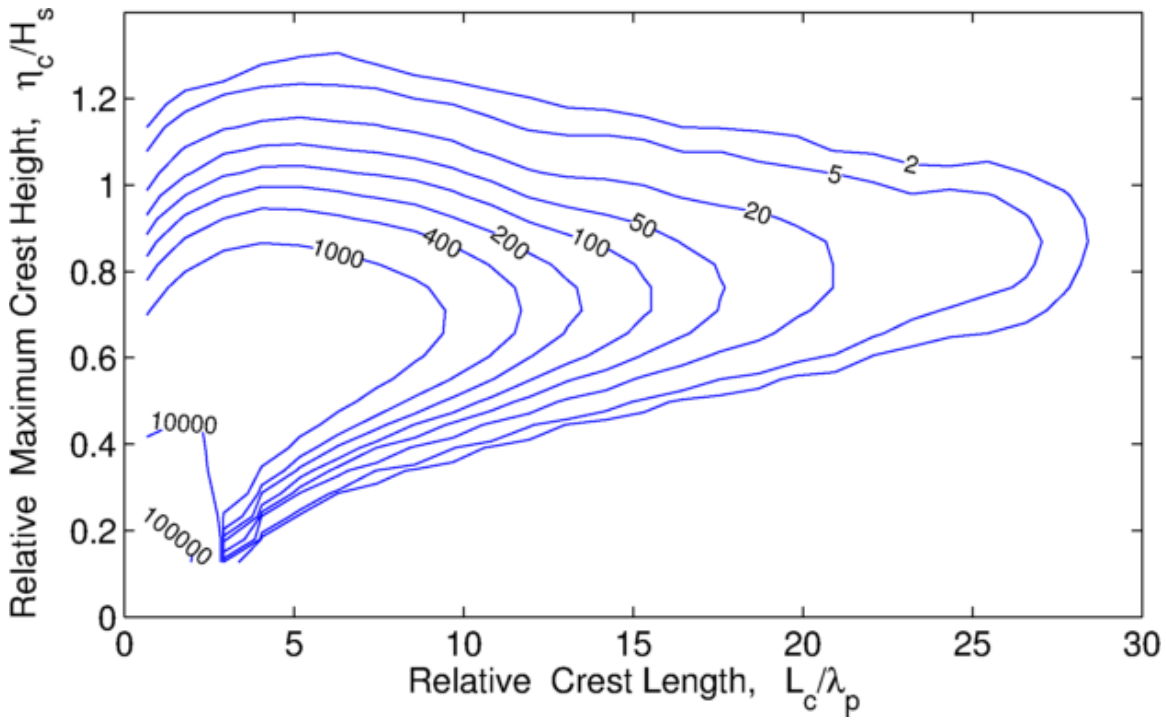

Figure 6-7 Joint distribution of relative crest length vs. relative maximum crest height.

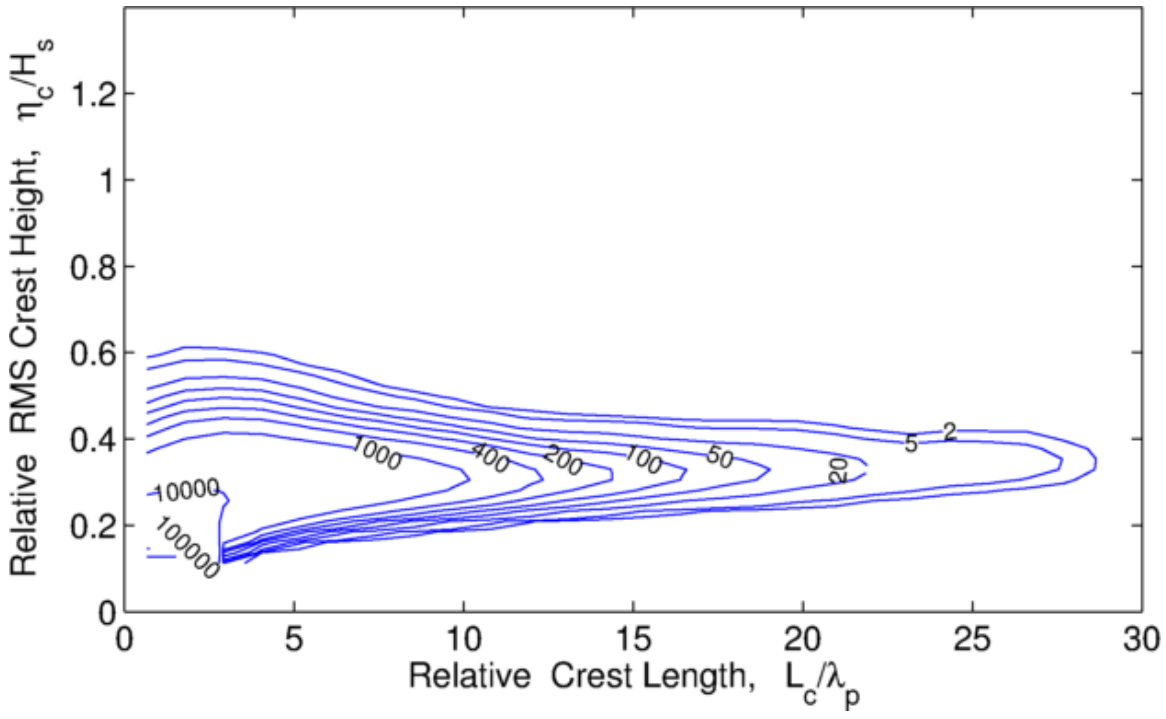

Figure 6-8 Joint distribution of relative crest length vs. relative rms crest height.

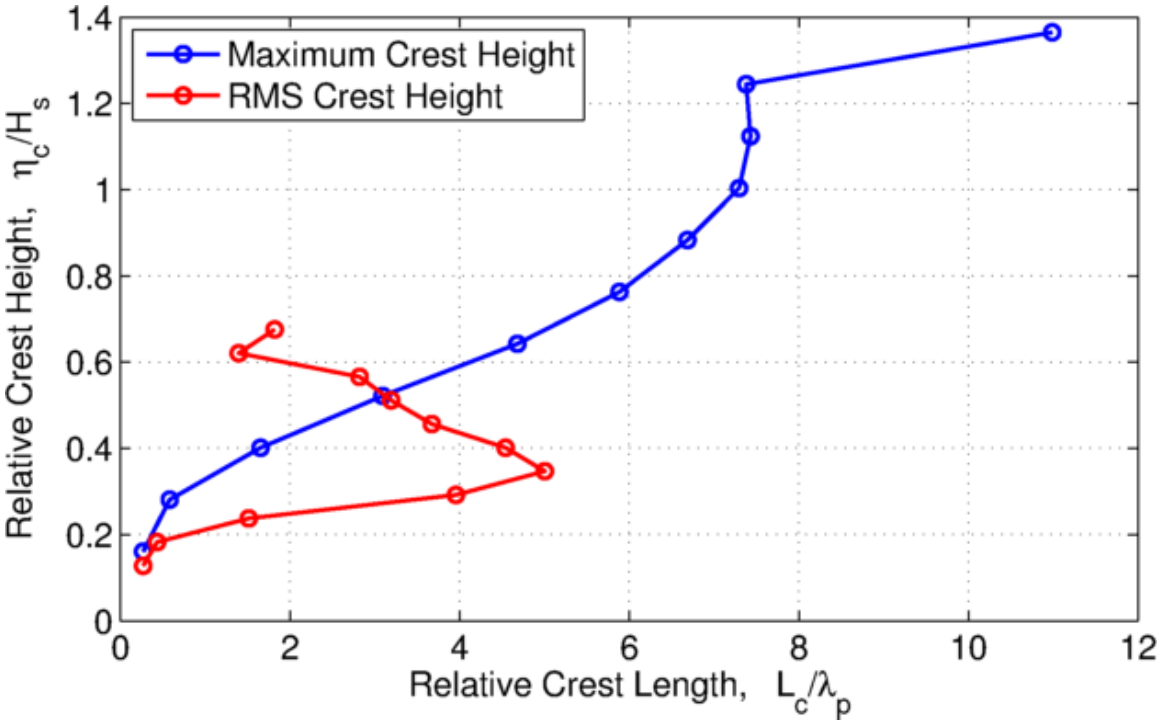

Figure 6-9 Relative wave crest heights as a function of relative wave crest length.

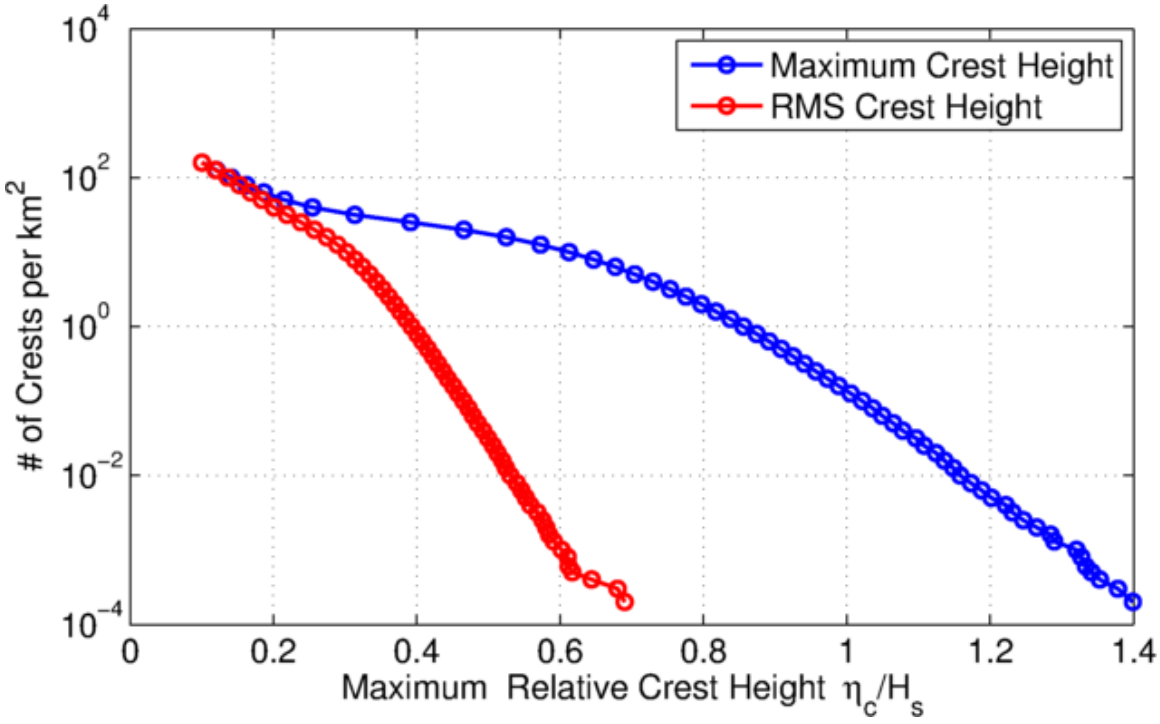

Figure 6-10 Distribution of wave crests exceeding a given relative crest height.

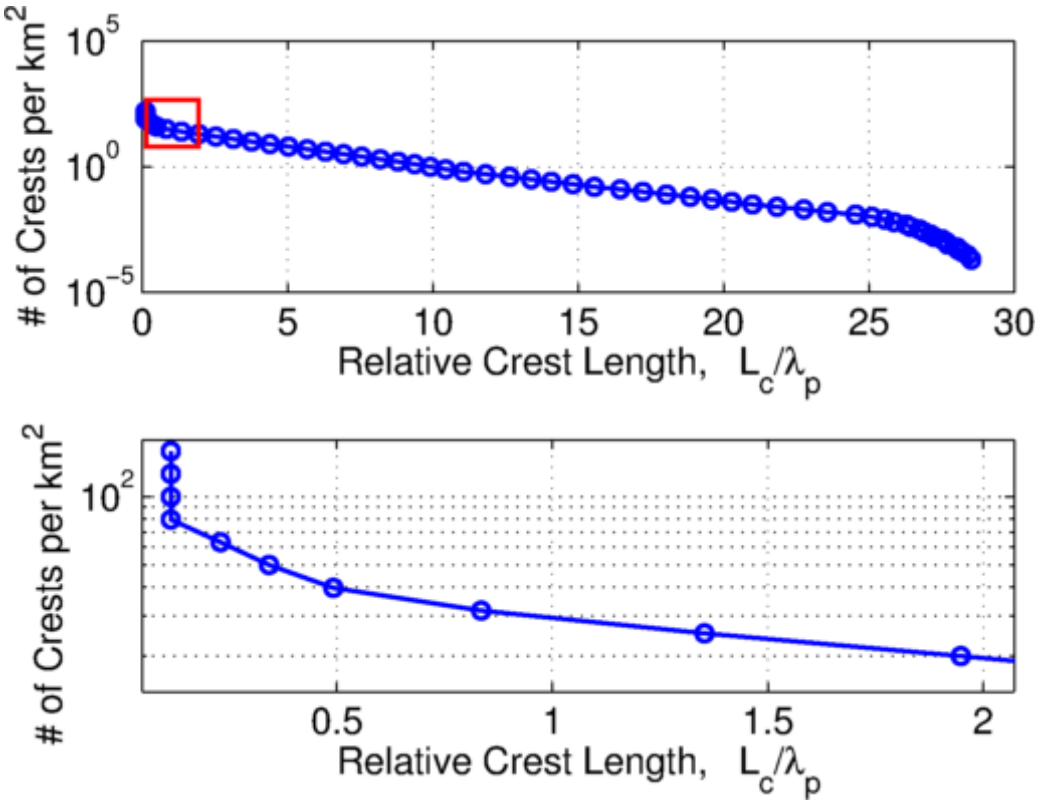

Figure 6-11 Top: Distribution of wave crests exceeding a given relative crest length. Bottom: Zoomed in to the section of the plot shown with the red box.

6.3 Simulation using Parametric Spectra

By varying wave period, peak shape parameter and spreading parameter 280 different sets of parameters were simulated with 50 repetitions each. The repetitions are required to get statistically representative values for the stochastic simulations. A constant significant wave height of 1 m was used. The sea surface was simulated over an area 1500m by 1500 m using an element size of 5 m. The crest threshold was set at 0.1 H_s and no additional filtering was used. Figure 6-12 through Figure 6-14 show the variation of the mean wave crest length L_c normalized by wave length, l, as a function of peak period T_p, the peak shape parameter, γ and Mitsuyasu directional spreading parameter sp_{max}. Wave crest lengths increase when sp_{max} increases (directional spreading decreases), and when γ increases (more energy around the peak frequency). The normalized wave crest length decreases with increasing T_p. This is due to normalization and the absolute value of the wave crest lengths increase. The relationships are not linear as seen in the shape of the contours.

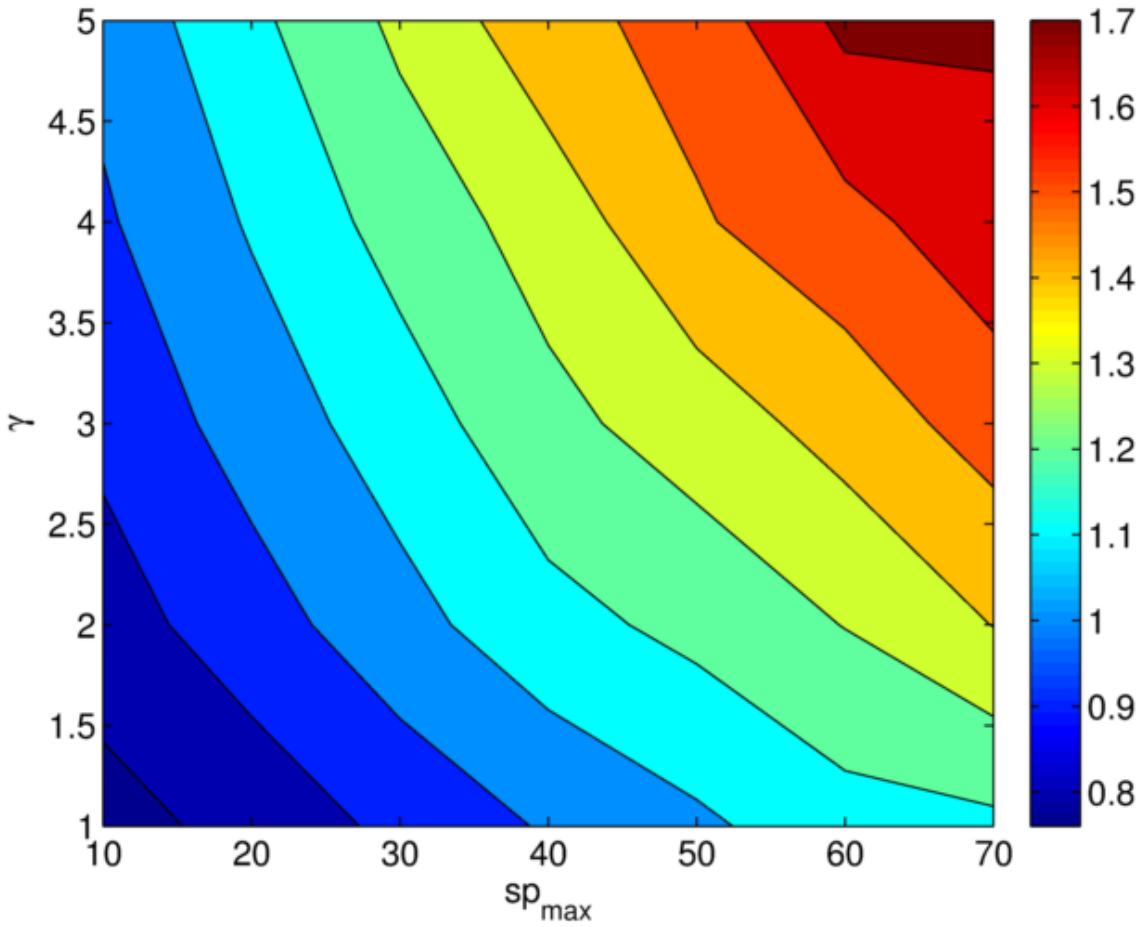

Figure 6-12 Contour plot of mean wave crest length normalized by wave length as a function of the spreading parameter sp_{max} and the peak shape parameter γ (T_p=4 sec).

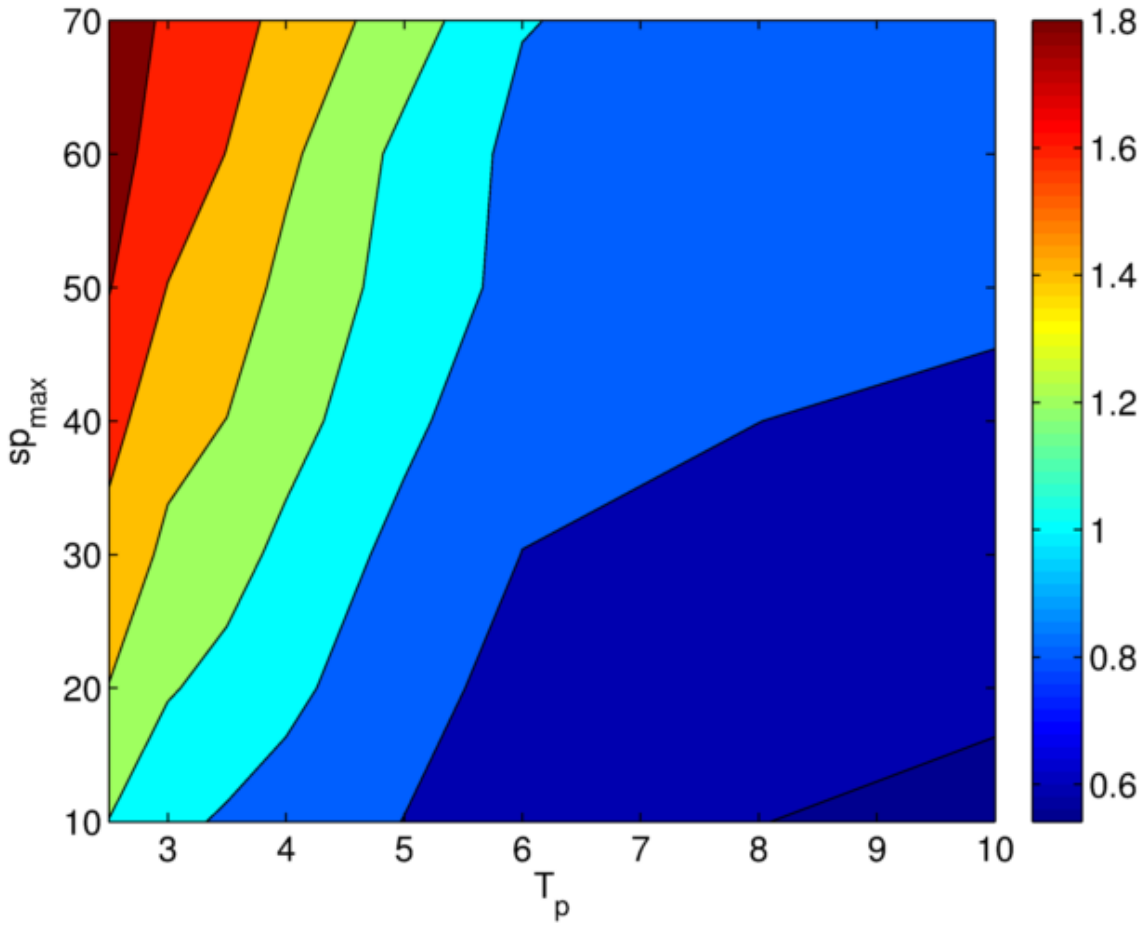

Figure 6-13 Contour plot of mean wave crest length normalized by wave length as a function of the peak period T_p and the spreading parameter sp_{max} (γ =3).

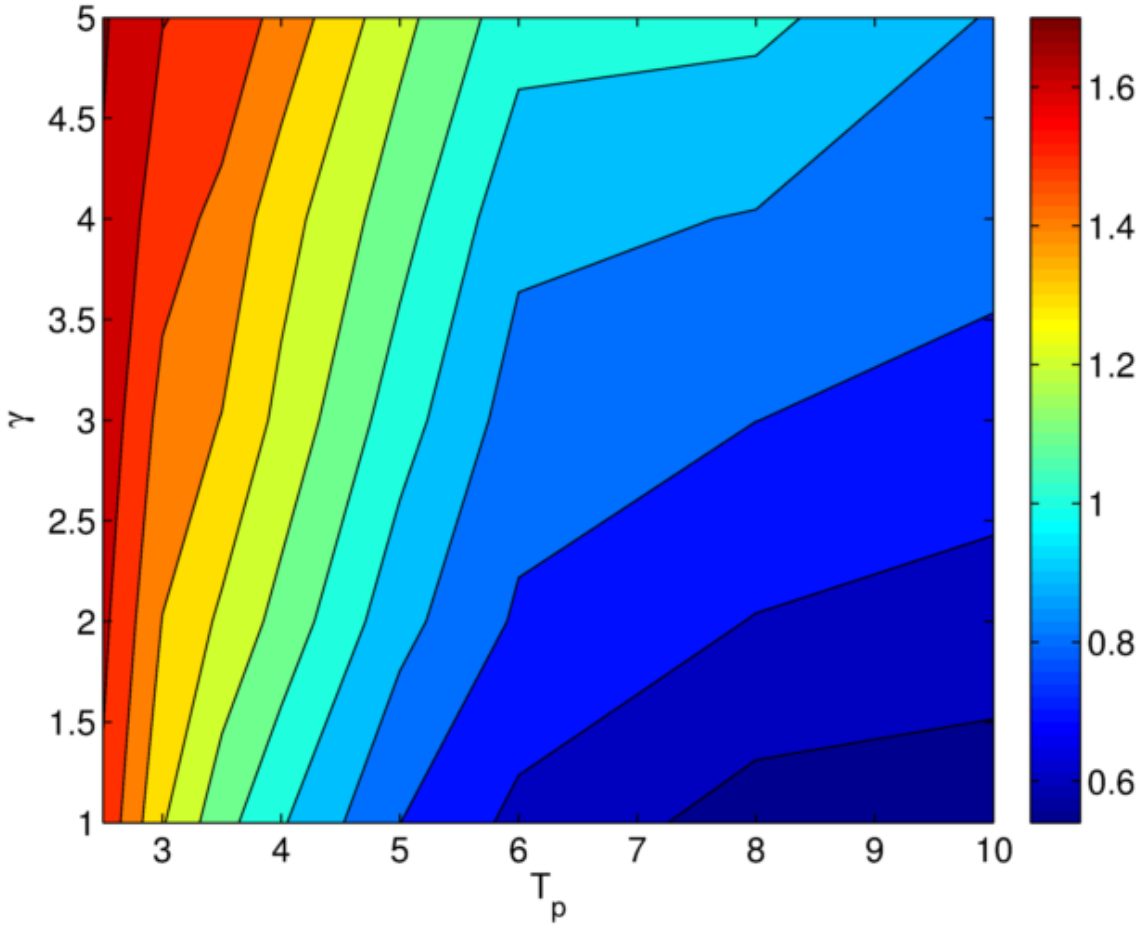

Figure 6-14 Contour plot of mean wave crest length normalized by wave length as a function of the peak period T_p and the spreading parameter γ ($sp_{max} = 40$).

6.4 Effect of Wave Nonlinearity on Wave Crest Lengths

This section discusses the effects of nonlinearities on wave crest lengths as well as the difficulties associated with nonlinear wave analysis. The sea surface simulations discussed thus far in this report have all used first order linear wave theory.

Longuet-Higgins (1963) was the first to develop the equations for second-order nonlinear interactions for waves in deep water. These equations were extended to waves in finite water depths by Sharma and Dean (1979). Forristall made minor corrections to Sharma and Dean's equations in 2000 (Forristall 2000). Romero and Melville (2011) showed that nonlinearity can have a significant effect on total wave crest lengths per unit area, however, the effects on wave crest length alone were not investigated.

For a given directional wave spectrum the effects of second order wave interactions can be calculated and added to the first order solution. All of the spectral bins interact with each other. For example for a spectrum with 40 directional bins and 50 frequency bins there are $(40*50)^2$ =4 million interaction terms. For a complete second order analysis, all interaction terms must be calculated at each time step and position. Even though there are methods to optimize these calculations, the computation time for a nonlinear analysis is

typically 2 to 3 orders of magnitude longer than that for an equivalent linear analysis. The simulations must to be repeated many times in order to have sufficient data for the statistical analyses which exasperates the problem.

An example of a nonlinear simulation is shown in Figure 6-15. The non-linear terms increase crest and trough elevations, but decrease the elevations elsewhere. The result is a more skewed sea surface, with larger crests and smaller troughs.

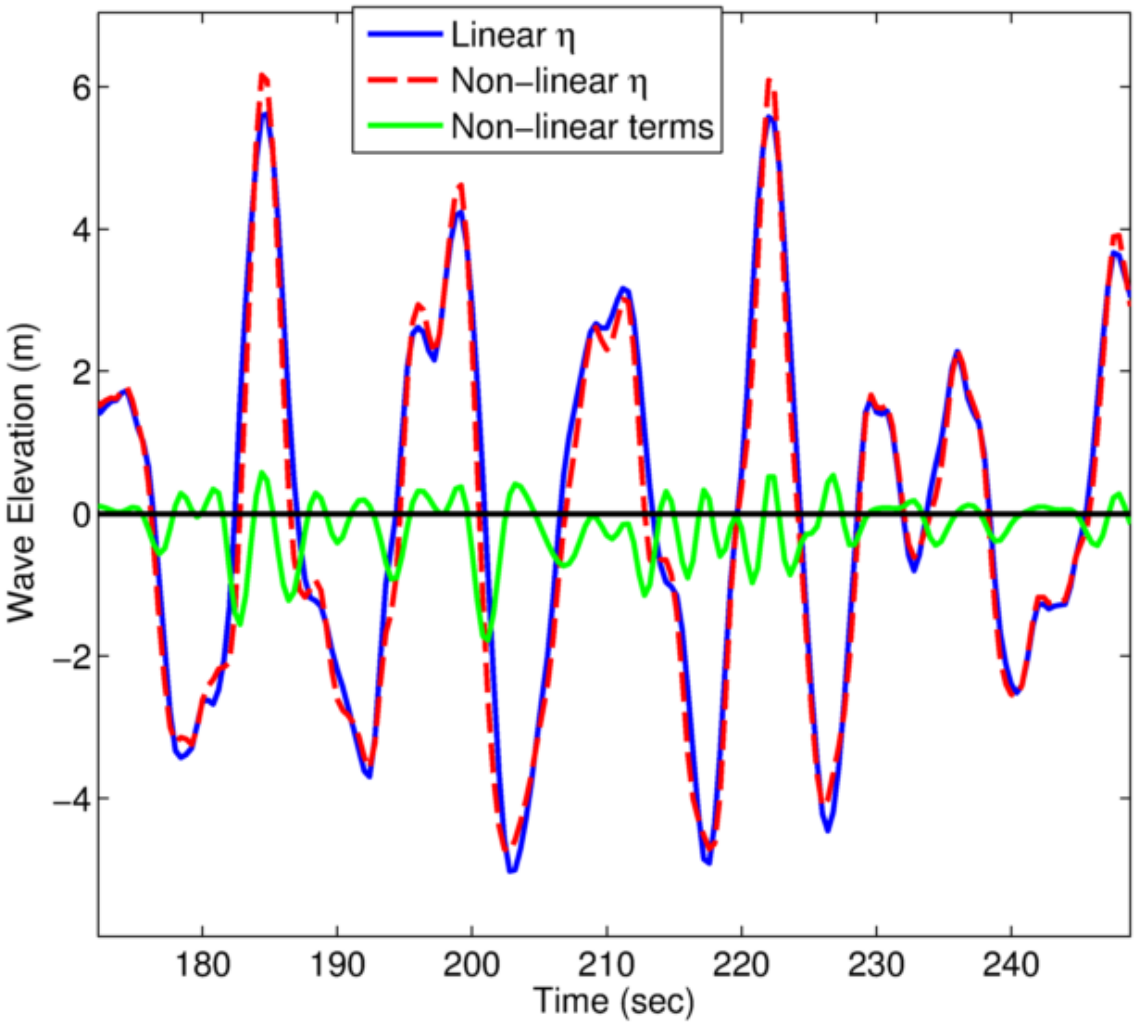

Figure 6-15 Example of second order non-linear wave surface simulation. JONSWAP spectra T_p=12 sec, H_s=11.2 m, water depth = 40 m.

The effects of nonlinearity on wave crest lengths depend on the threshold chosen in the analysis. If a low threshold is chosen the wave crest lengths will be shorter, because as seen in Figure 6-15 non-linearity depresses the sea surface around the still water line. Note that even though Figure 6-15 is a temporal plot, a spatial plot would be similar. This can be seen by looking at the argument of the cosine term in Equation (11). The non-linear surface will have longer crest lengths only for higher thresholds.

Mean crest lengths are compared for linear and non-linear simulations in Figure 6-16. Regardless of the threshold value, linear simulations have longer crest lengths, which is not expected. The reasons become clear in Figure 6-17, which shows the case with a threshold value of $0.8H_s$. Non-linearity increases the longest wave crest lengths, but it also adds many more waves with small crest lengths creating a net decrease in the overall mean crest length. Comparing the larger crest lengths gives a better picture of the effects of non-linearity. The use of significant wave height (mean of highest one third of the values) is not appropriate since a definition that is not dependent on the smaller wave heights is needed. Mean of the highest 10 crest lengths were chosen as the parameter used for comparison. This does not translate to anything meaningful in another setting, but can be used to compare the two cases. The ratios of non-linear to linear crest lengths are plotted in Figure 6-18. The blue curve shows the same information as Figure 6-16 and the red curve is the mean of the highest 10 wave crests. Except for the smallest threshold, the non-linear crest lengths are higher than the linear crest lengths when only the longer crest lengths are taken into account.

Non-linearity alters wave crest elevations too. Even for the top 10 wave crest elevations the non-linearity increases crest heights less than 10% (Figure 6-19). In the literature threshold values varying between 0.10 and 0.25 have been used. The choice of this value has much greater influence on the crest lengths than the effects of non-linearity (Figure 6-16). The influence of non-linearity is small compared to the effects of other parameters investigated in this study. However the computational requirements for non-linear simulations are huge. Linear simulations were used in this study. The effects of non-linearity were included as a correction factor as explained in the next section.

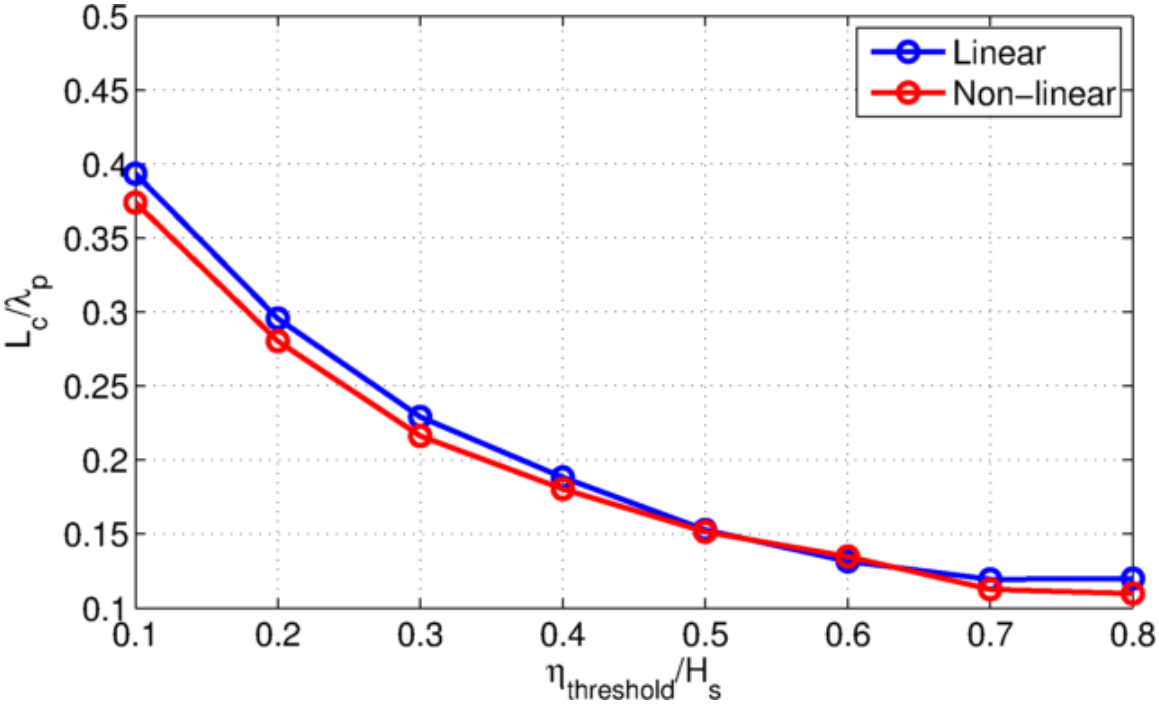

Figure 6-16 Comparison of mean crest lengths as a function of threshold value.

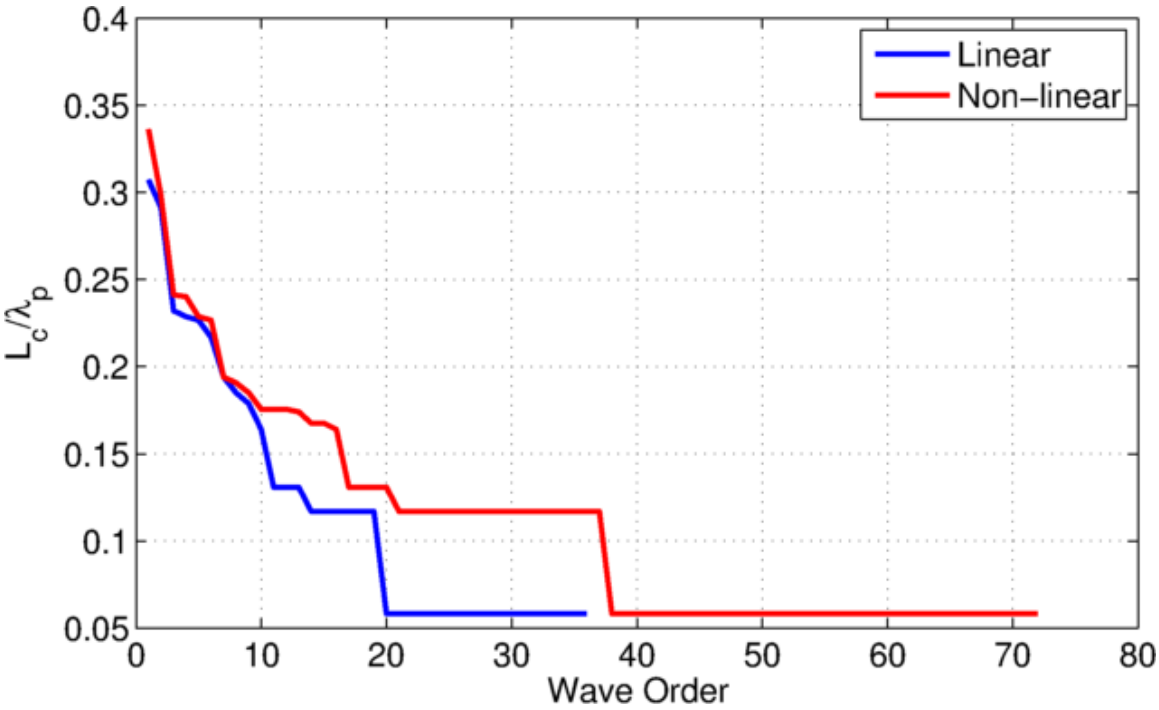

Figure 6-17 Mean wave crest lengths sorted in descending order. The threshold is 0.8 H_s.

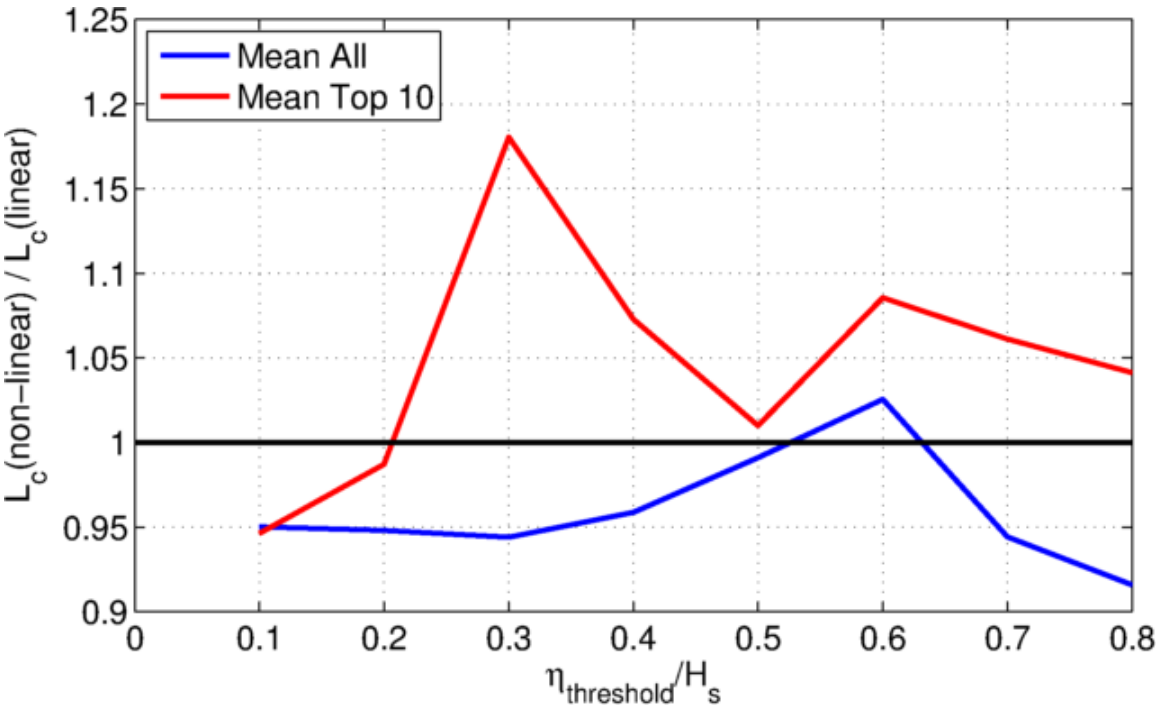

Figure 6-18 Ratio of non-linear to linear crest lengths as a function of the normalized threshold value.

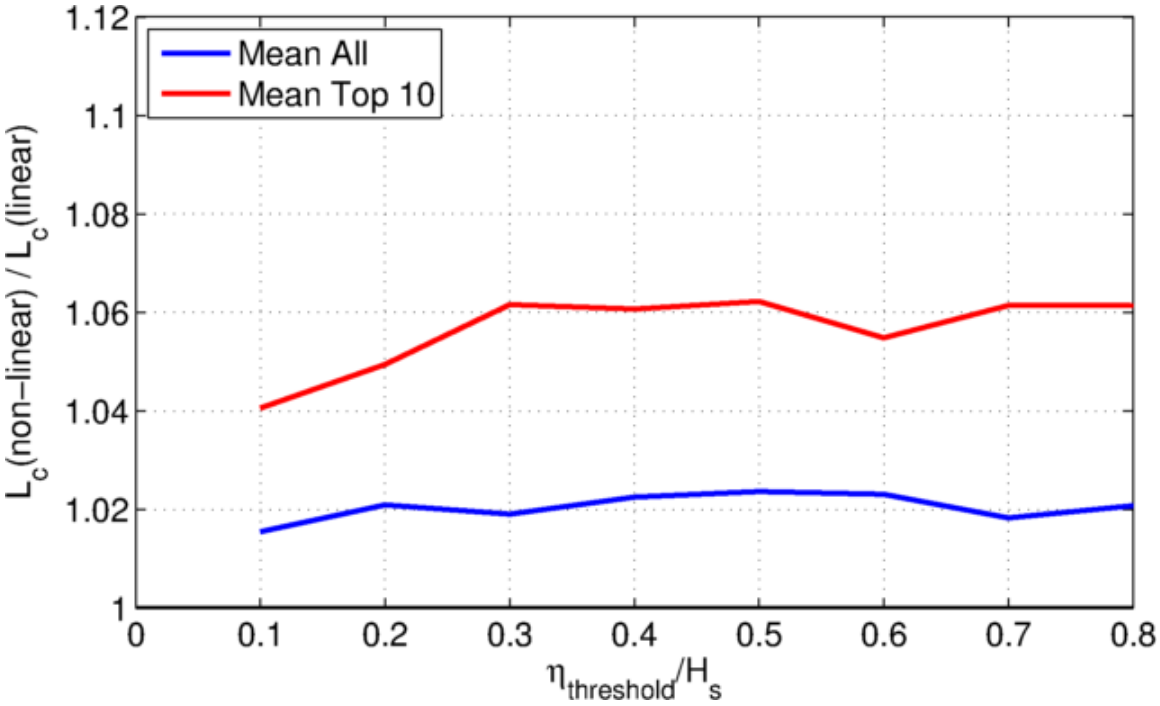

Figure 6-19 Ratio of non-linear to linear crest heights as a function of the normalized threshold value.

7.0 Corrections Based on Measured Sea Surface Data

Various sources for sea surface measurements have been identified. However, all are for open, deep water conditions. No shallow water data in enclosed bays were located. All of the data sets have very limited quantities of data. Even if all of the existing data was obtained and combined; the quantity would still be too small to be of value to this study. Developing predictive equations for the differences between wave crest lengths obtained from sea surface images requires a significant quantity of data. Additionally different data sets were collected with different measurement techniques and analyzed using different methodologies. The data would need to be reprocessed to have a consistent data set.

The differences between real and simulated sea surfaces have been quantified using Monaldo (2000) data. He presents eleven different plots similar to Figure 6-11 showing the number of waves with wave lengths exceeding a given value. He had both simulated and measured sea surface data. The measured data consisted of eight measurements during Hurricanes Josephine in 1984 and three measurements during Hurricane Bonnie in 1998. Design wave crest lengths (25% exceedance probability as found in Chapter 6.2) were obtained from the simulated and measured sea surface plots . The ratio of measured wave crest length to simulated crest length is shown in Figure 7-1. The first eight are from Hurricane Josephine and the last three are from Hurricane Bonnie. The ratios vary from 0.8 to 1.5 with an average value of 1.15 (dashed blue line) and all but one are less than 1.3. These differences include both non-linear effects and phase correlations between phases that are not included in (random phase) simulations. These results are consistent with the non-linear analysis results which are on the order of 10%. A safety factor SF_M of 1.30 was chosen to account for all of the effects that are not in the sea surface simulations.

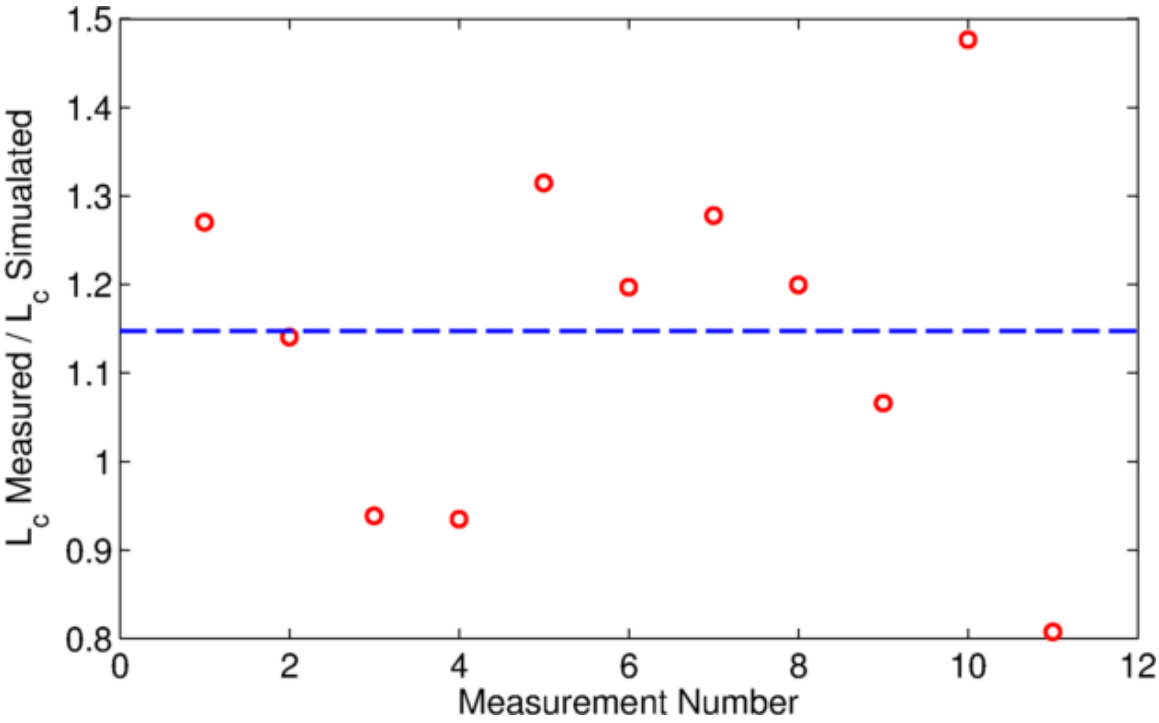

Figure 7-1 Ratio of crest lengths obtained from measurements to simulated sea surfaces. The dashed blue line shows the average.

8.0 Effects of 3D Sea Surfaces on Wave Forces

Attempts to establish a meaningful definition of wave crest length for a given location and sea state were hampered by the arbitrariness of the threshold value needed to define the crest length. That is, at what level above the still water surface should be chosen to define the crest. Figure 8-1shows the effect the threshold has on wave crest length. Additionally more arbitrary filtering parameters were required to filter out very small waves. These issues motivated the development of a different approach to the problem that is directed at the application of interest in this study, namely storm surge/wave loading on bridge superstructures. This approach not only eliminates the need to define a threshold but takes the variation in crest height and its impact on the wave forces on the bridge superstructure as well.

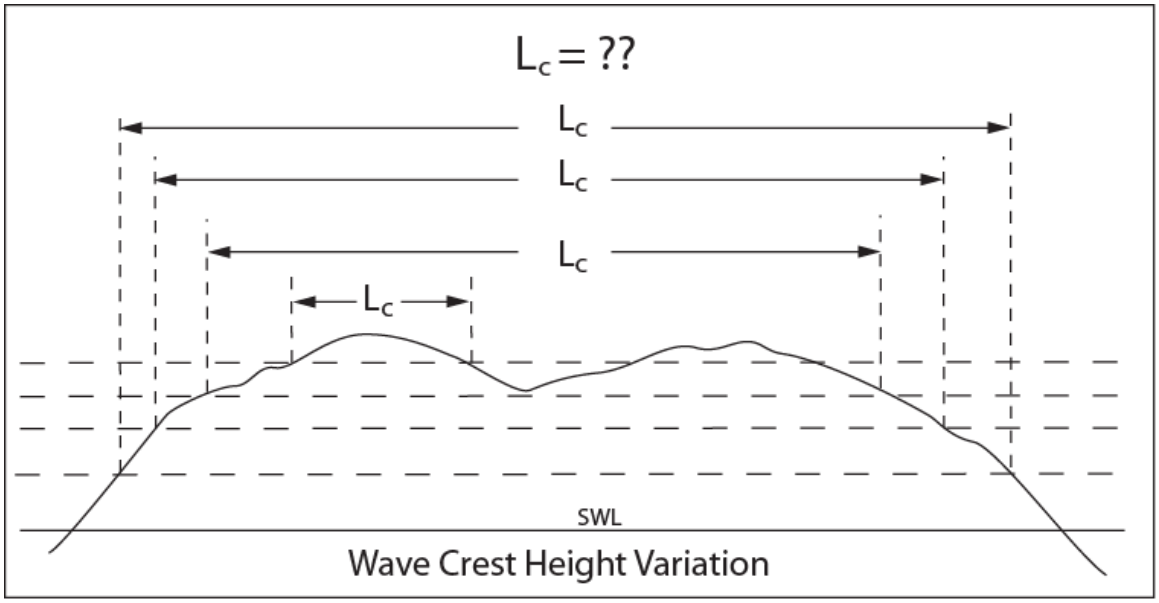

Figure 8-1 Figure showing the impact of threshold value on wave crest length.

The current procedure for computing the "design wave height" is to multiply the significant wave height, H_s associated with the design event by 1.8. The 1.8 value corresponds to a 0.015 probability of exceedance. A methodology to account for the effect of wave crest height variation along the crest on wave forces imparted to a horizontal structure, like a bridge span, was developed which adjusts the value of the 1.8 multiplier. Using a 1.8 multiplier assumes that wave heights do not vary along the wave crest and the wave crest length is larger than the span length. These assumptions are too conservative most of the time since wave crests vary in height along the crest as shown in Figure 8-2. Only a portion of the span may be impacted by the wave depending on the crest height variation and the span elevation and length.

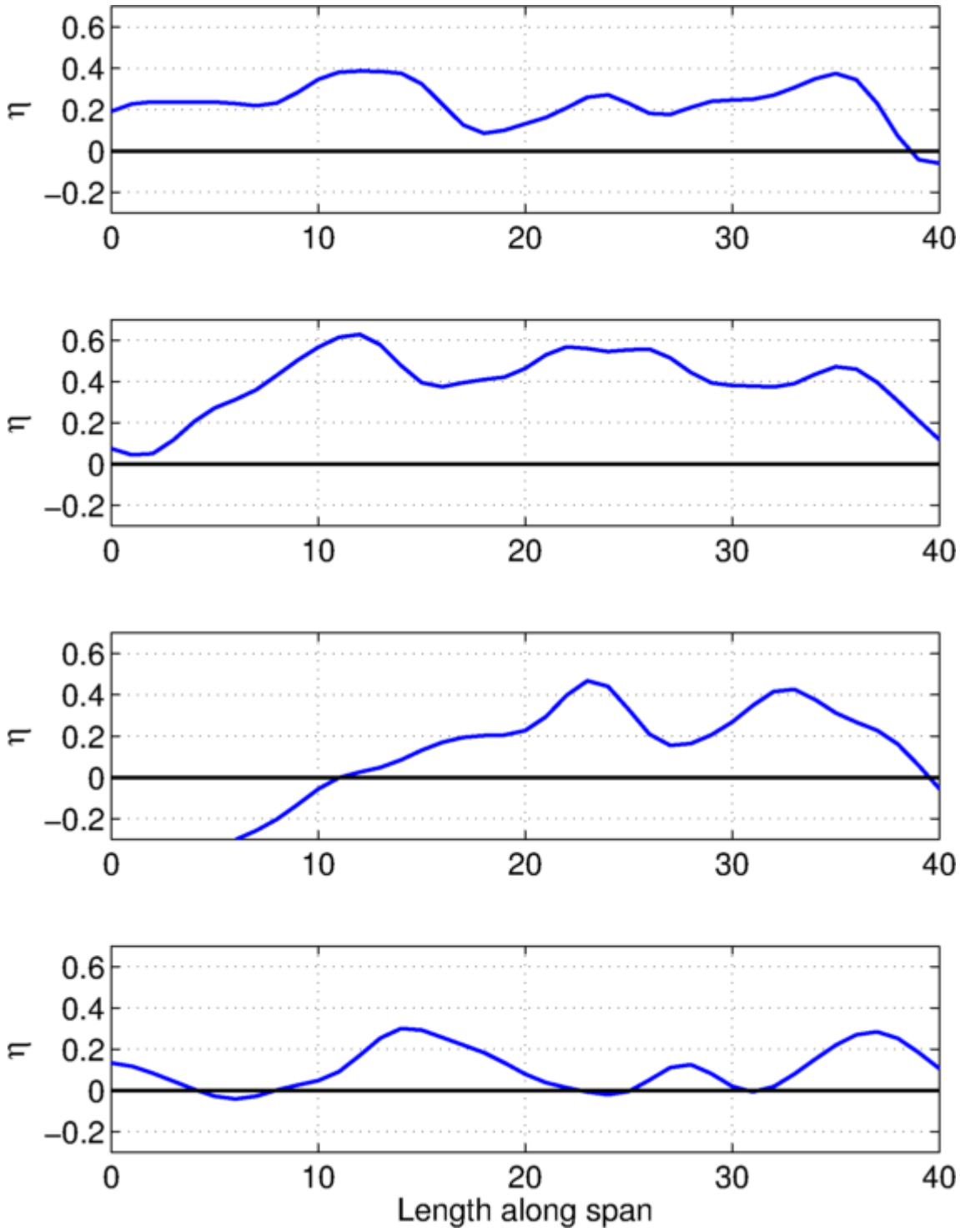

Figure 8-2 Sea surface η along a bridge span at different times.

This method takes advantage of the fact that vertical wave forces, F_z vary linearly with wave height. Figure 8-3 and Figure 8-4 show this for a slab span and a girder span respectively. These forces were calculated using the PBM (computer program for computing wave forces on bridge superstructures), which was used to generate the data

used to develop the parametric force equations in the AASHTO document.. Since wave forces vary linearly with wave height, wave heights observed at a bridge span can be averaged to come up with a representative wave height and calculate a multiplier to replace the1.8 value in the AASHTO document. The new procedure is summarized below:

Input Parameters: Wave spectra, bridge span length, L_s, and bridge span clearance z_c.

1. Simulate sea surface elevation at the bridge span $\eta(x,t)$
2. Apply zero crossing analysis to η to identify crests.
3. Check all the identified waves for steepness decrease η for waves that exceed the steepness criteria.
4. At each time step identified as a crest, calculate the average η including only portions touching the bridge and calculate a representative wave height $H_i = 2\overline{\eta}_{crest}$
5. Calculate $(C_1)_i$, the portion of the span that is touched by the wave crest
6. Repeat steps 4 and 5 at least 4000 times to get statistically robust results.
7. Find the wave height exceeded by only 0.15% of H_i. Define $C_0=H_i(0.15\%) / H_s$
8. Find the associated $(C_1)_i$ and define that as C_1.
9. Calculate Preliminary Wave Force using $(C_0/C1)\ H_s$ and instead of $1.8H_s$ as the design wave height in the wave force calculations.
10. Calculate final wave force as C_1*Preliminary Wave Force

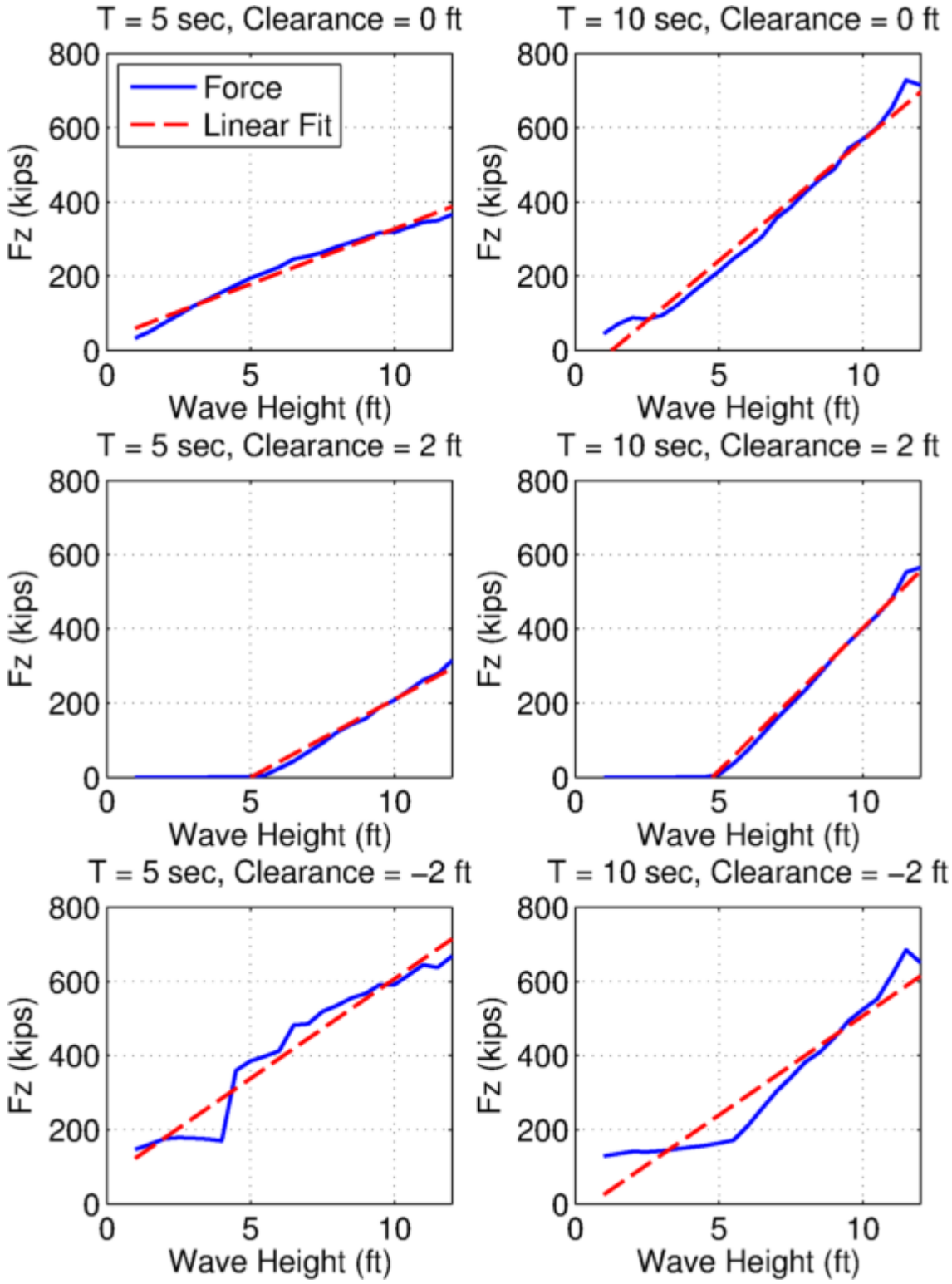

Figure 8-3 Wave forces calculated with PBM as a function of H_s, z_c and T_p for a slab span (length=50 ft, height 1 ft).

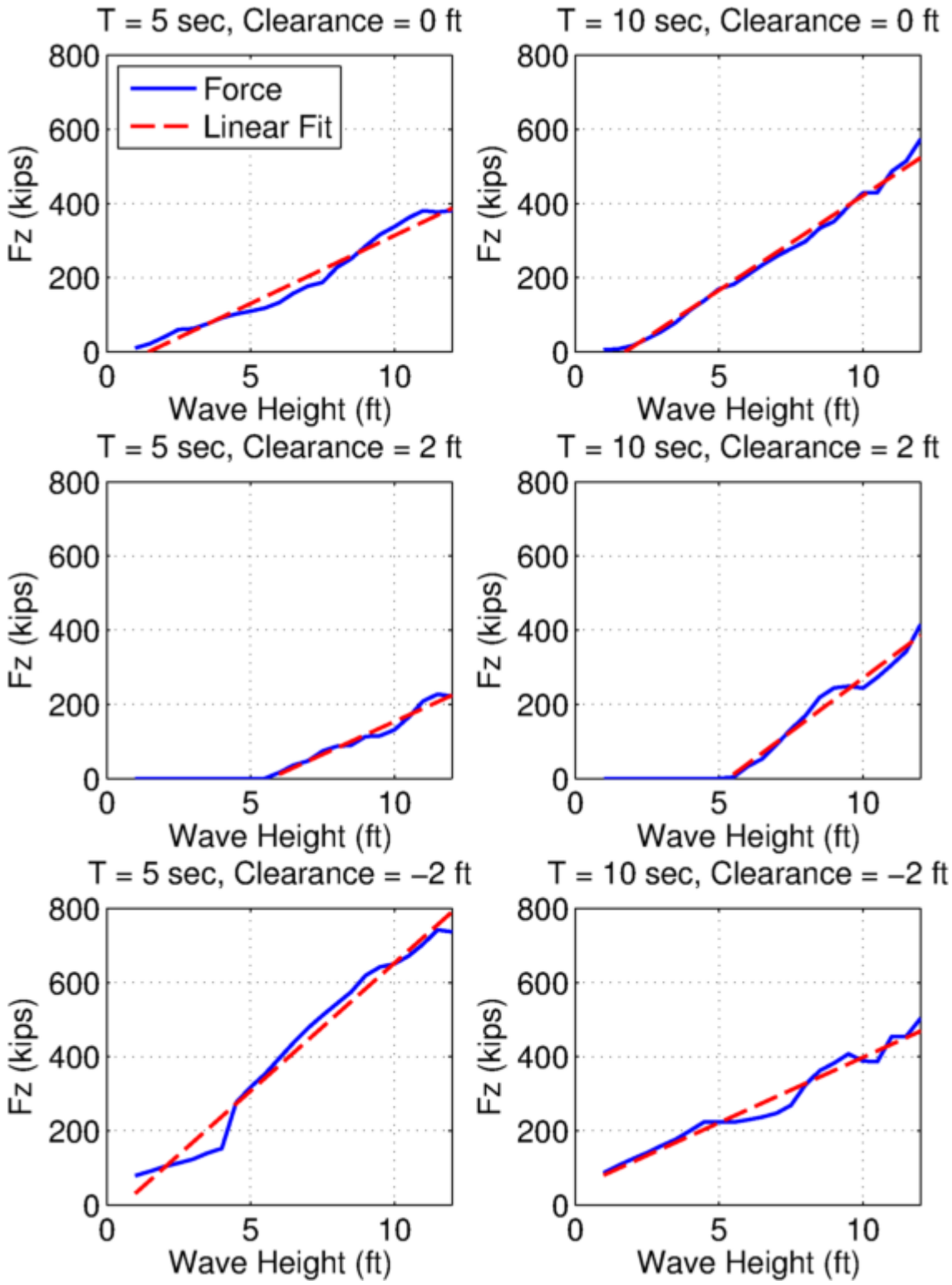

Figure 8-4 Wave forces calculated with PBM as a function of H_s, z_c and T_p for a girder span (AASHTO Type III, length 50 ft).

8.1 Empirical Equations for Predicting 3D Sea Surface Effects

Simulation of sea surfaces is a complex procedure and also requires the availability of wave spectra. The direct simulation technique will not feasible most of the time. As alternative, empirical equations were developed that predict the coefficients C and C_1 based on limited amount of wave parameters. In order to establish the feasibility of this approach it was decided to only include maximum wave height depth and steepness limitations after the fact to make the analyses tractable for this study. This is discussed further in the conclusions. With this in mind the met/ocean parameters analyzed for their influence on C are shown in Table 7-1 along with a qualitative assessment of C's dependence on the parameter.

Table 8-1 Wave force sensitivity analysis results.

Variable	Symbol	Effect
Significant Wave Height	H_s	Significant
Wave Length	λ	Significant
Water Depth	h	Small
Directional Spreading	D_{spr}	Significant
Peakedness parameter	Q_p	Small
Span Length	L_s	Significant
Freeboard	z	Significant

Initially two common wave spectra, JONSWAP and TMA were used in the analysis. Physically meaningful groupings of the parameters were developed and used as independent variables in the empirical equations. The resulting empirical equations (developed from sea surface simulations produced from JONSWAP and TMA spectra) were calibrated and tested using SWAN generated spectra for coastal waters in North Carolina. More than 6000 sea surface simulations based on SWAN spectra and more than 5000 sea surface simulations based on JONSWAP and TMA were used. Each sea surface was created more than 4000 times for statistical stability. In total more than 40 million simulations were performed.

The following parameter groupings were used in the empirical equations:

$$\begin{aligned} \alpha &= \left(\frac{L_s}{\lambda}\right) D_{spr} \\ &= \left(\frac{\text{span length}}{\text{wave length}}\right) (\text{directional spreading angle in degrees}) \end{aligned} \tag{13}$$

$$z' = \max\begin{cases}\dfrac{z_c}{H_s}\\ 0\end{cases} \qquad (14)$$

$$= \left(\frac{\text{clearance (distance from design water level to span low chord)}}{\text{significant wave height}}\right)$$

The equation to calculate the required coefficients are below:

$$C_0 = K_z\left[1.8 - \tanh\left(\frac{0.0122\alpha}{SF_E SF_M}\right)\right]$$

where

$$K_z = \max\begin{cases}\tanh\left(\dfrac{1.208 - z'}{1.451 z'^{14} + \tanh\left(0.01974 z'\ \alpha\right) + \dfrac{0.08495}{\left(1.208 - z'\right)}}\right)\\ 0\end{cases} \qquad (15)$$

K_z a measure of the effect of the clearance and

SF_E is a safety factor that accounts for errors in the empirical equation and is equal to 1.2

SF_M is a safety factor that accounts for errors in the sea surface simulations and is equal to 1.3

Note that even though the safety factors are large ($SF_M SF_E$=1.56), their effect on C_0 is much smaller as seen in Figure 8-5. The maximum increase in C_0 is 20% for α=100 while for a more typical value of α=20 increase in C_0 is only 5%. The effects on wave forces will be similarly small.

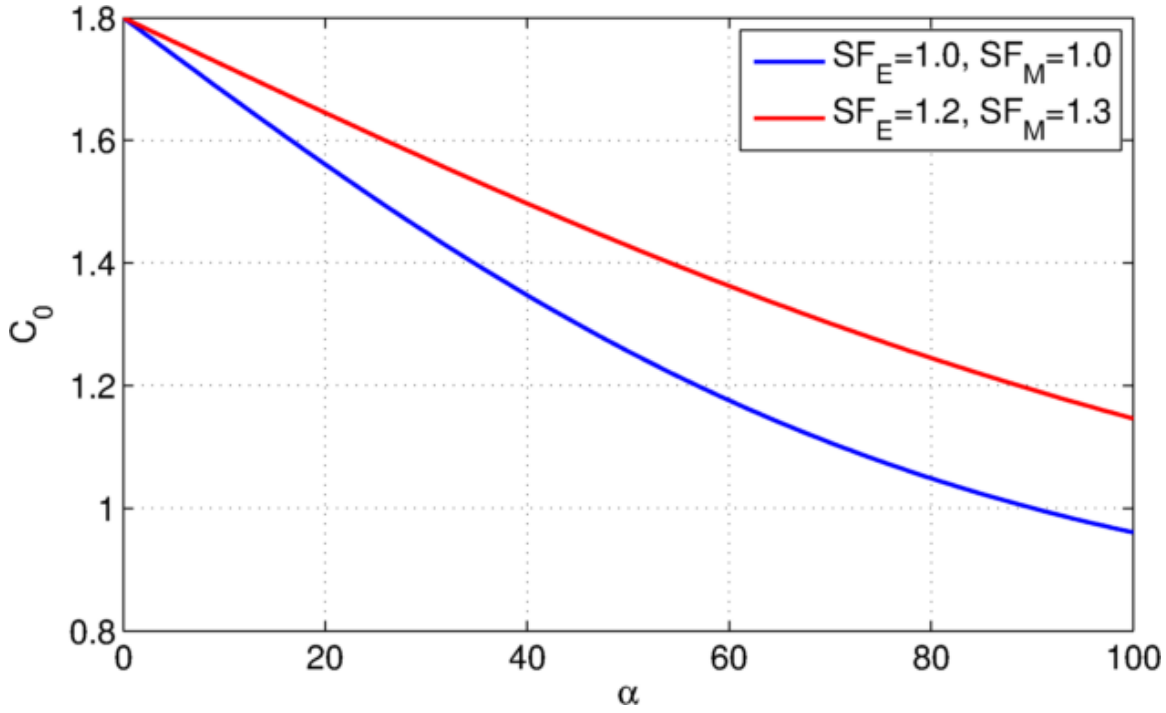

Figure 8-5 Effect of safety factors on C_0 assuming K_z=1

C_1' is the ratio of impacted span length over actual span length.

$$C_1' = \max\begin{Bmatrix} \tanh\left(0.06072 + \dfrac{(32.88 - 34.32z')}{(z'\,\alpha + 11.22z'^{5})}\right) \\ 0 \end{Bmatrix} \tag{16}$$

Note that for submerged spans z'=0, K_z=1 and C_1'=1.The wave height that is to be used in computing the vertical force on the span (assuming the entire length of the span is impacted by the wave) is:

$$
\begin{aligned}
&T_{SF} = SF_T T_p \\
&SF_T = 1.2 \\
&C_U = \frac{2\pi 0.02 \lambda_{T_{SF}} \tanh\left(\frac{2\pi}{\lambda_{T_{SF}}} d_s\right)}{H_s} \\
&C = \min \begin{cases} \dfrac{C_0}{C_1'} \\ 2.5 \\ C_U \end{cases} \\
&H_{input} = CH_s
\end{aligned}
\tag{17}
$$

where d_s is the water depth including surge and λ_{TSF} is the wave length calculated using T_{SF} as the wave period. Safety factor SF_T used in the calculation of T_{SF} is required because when waves are steepness limited periods associated with design wave heights increase, C is controlled by steepness and safety factors used in the calculation of C_0 has no effect. The period that will be used in the wave force calculations T_{input} is calculated using

$$
\begin{aligned}
&T_{input} = \begin{cases} \mathrm{T_{SF}} & \text{if} \quad \mathrm{C=C_U} \\ T_{\mathrm{int}} & if \quad C_L > C > C_U \\ T_p & C < C_L \end{cases} \\
&C_L = \frac{2\pi 0.02 \lambda_p \tanh\left(\frac{2\pi d_s}{\lambda_p}\right)}{H_s} \\
&T_{int} = \frac{1}{\tanh\left(\frac{2\pi}{\lambda_{int}} d_s\right)} \sqrt{\frac{H_{input}}{0.02g}}
\end{aligned}
\tag{18}
$$

Note that the expression for T_{int} is implicit and needs to be solved iteratively since λ_{int} is a function of T_{int}. For shallow water steepness limited criteria is equivalent to $H/d_s=0.79$, which is very close to $H/d_s=0.78$ derived based on solitary waves and generally used for depth limited waves. As a result a separate depth limited criteria is not needed. It should be noted that the equation 6.2.2.4-9 in AASHTO specifies a depth limitation of $H/d_s=0.65$. This value is applicable to significant wave heights, but it can be exceeded by individual waves and should not be used for design wave heights. The preliminary force

is calculated by using H_{input} and T_{input} as inputs into the PBM or parametric wave force equations:

$$\text{PF} = \text{Preliminary Force (computed using } H_{input}, T_{input})$$

In order to account for cases where the entire span length is not impacted by the wave the vertical wave force computed using H_{input} in the vertical wave force equations must be multiplied by the ratio of impacted span length over actual span length, C_1, where

$$C_1 = \min\left\{\begin{matrix}\frac{C_0}{C} \\ 1\end{matrix}\right\}$$

The total force on the span becomes

$$\text{Force} = C_1 \text{PF}$$

Note that if the entire span length is impacted by the wave then $C_1 = 1$ and Force = PF.

PBM calculates non-linear wave surfaces based on stream function theory and the parametric equations require non-linear wave properties. However, the wave crest length analysis presented here assumes linear waves and wave lengths should be calculated using linear theory. The non-linear effects are included through the use of the safety factor SF_M.

Figure 8-6 and Figure 8-7 show the values of the coefficient C_0/K_z computed using JONSWAP and SWAN spectras respectively. SF_M and SF_E were taken as 1.0 in both cases. The fit is much better for JONSWAP spectra as expected. There is a small bias in the JONSWAP fit, because the coefficients in Equation (15) were optimized for the SWAN simulations.

Since there are thousands of data points in Figure 8-7, the points around the perfect fit line are being overlaid thus giving a somewhat exaggerated impression of the error. In Figure 8-7, 90% of the data points are within the dashed lines. Mean absolute error is 0.03 and the rms error is 0.045. Both of these numbers are less than 4% of the range of predicted values. There are some large outliers in Figure 8-7. Investigation of these outliers showed that these are mostly due to spectra with double peaks, which cannot be quantified with the existing parameterization. Figure 8-8 shows the same data with SF_E=1.2 used in the empirical equation. A little more than 5% of the data points are underpredicted with the empirical equations when the safety factor is used.

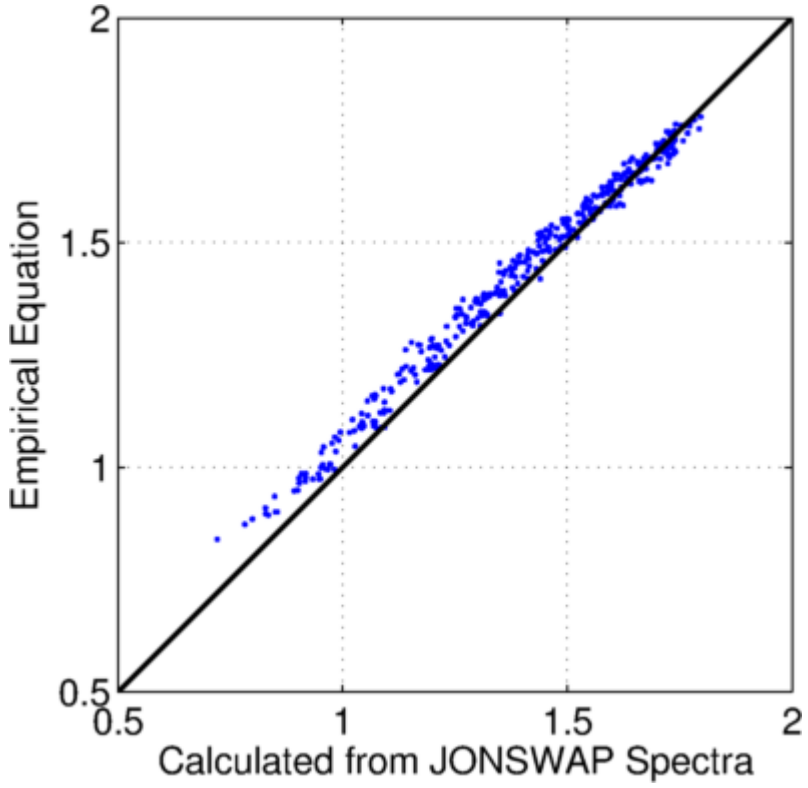

Figure 8-6 Coefficient C_0/K_z calculated from JONSWAP spectra vs. empirical equations

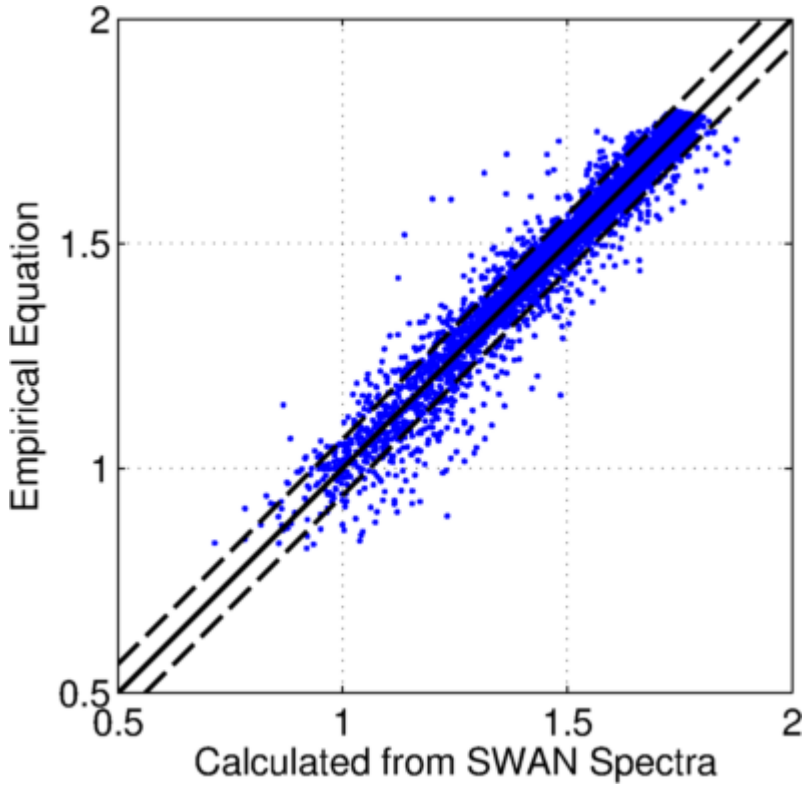

Figure 8-7 Coefficient C_0/K_z calculated from SWAN spectra vs. empirical equations. Solid line is the perfect fit, 90% of the data points are between the dashed lines.

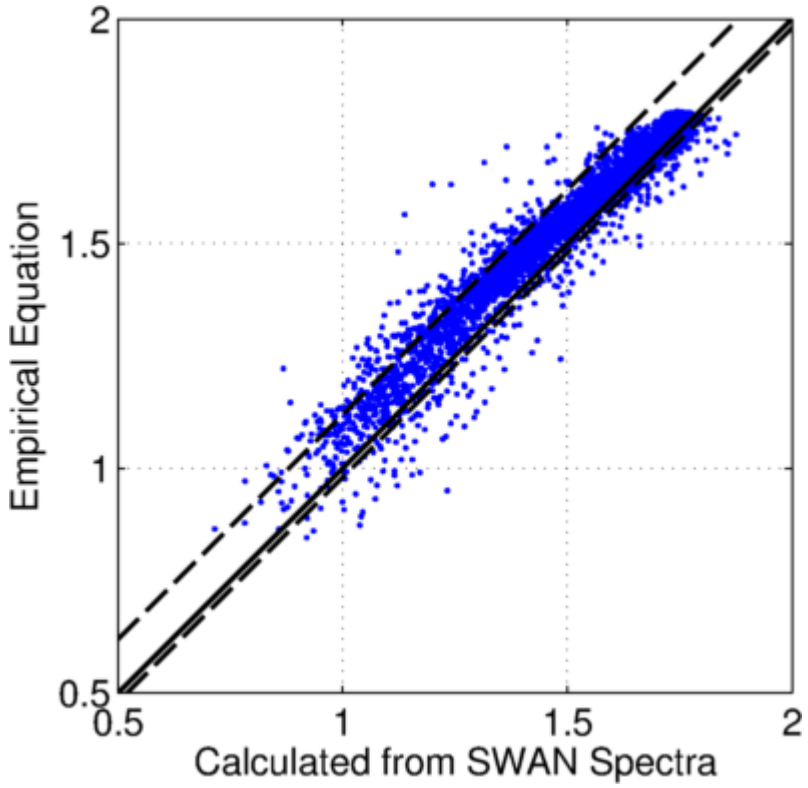

Figure 8-8 Coefficient C_0/K_z calculated from SWAN spectra vs. empirical equations with safety factor SF_E of 1.20. Solid line is the perfect fit, 90% of the data points are between the dashed lines.

The equations for K_z and C_1' were developed using JONSWAP spectra. Comparisons between the values of K_z and C_1' computed using the equations and obtained from sea surface simulations are shown in Figure 8-9 and Figure 8-10 respectively. The errors for the empirical equations are summarized in Table 8-2. All the errors are less than 5% of their associated ranges.

Table 8-2 Errors for the empirical equations for C_0, K_z and C_1'.

	Mean Absolute Error	**Root Mean Squared Error**	**Bias**
C_0/K_z SF_E=1	0.030	0.045	0.005
C_0/K_z SF_E=1.2	0.044	0.060	0.037
K_z	0.016	0.027	0.000
C_1'	0.011	0.018	0.001

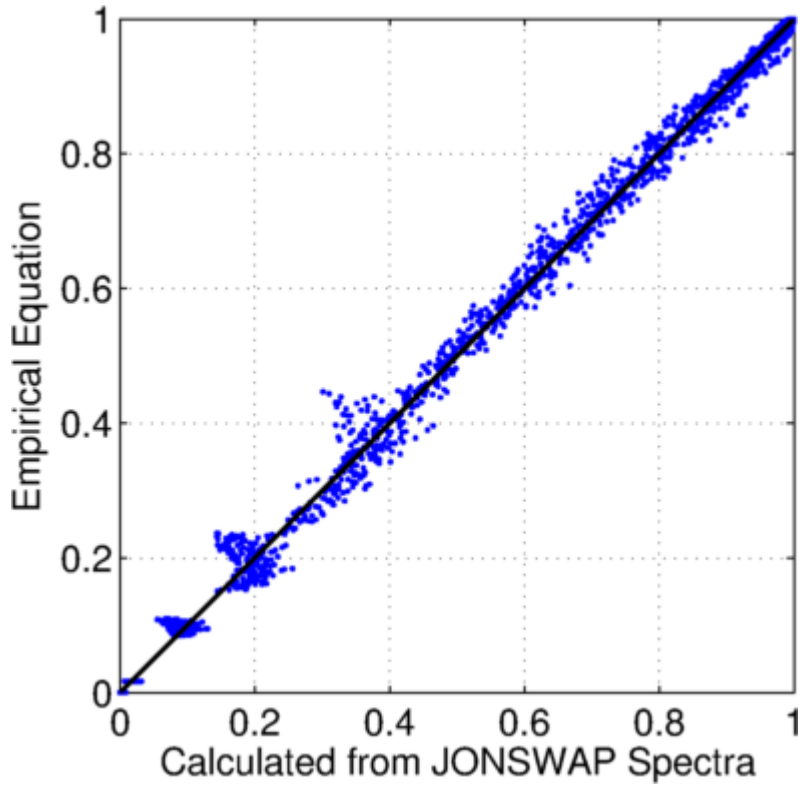

Figure 8-9 Coefficient K_z calculated from JONSWAP spectra vs. empirical equations

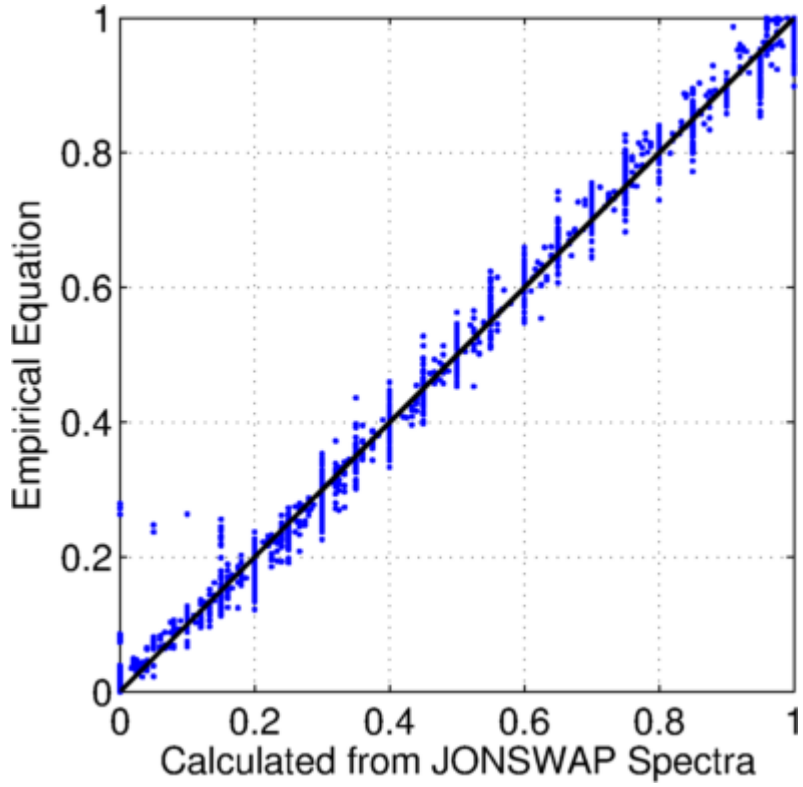

Figure 8-10 Coefficient C_1' calculated from JONSWAP spectra vs. empirical equations

Figure 8-11 and Figure 8-12 show K_z and C_2' as a function of normalized clearance z'. The solid lines are from simulations and dashed lines are from the empirical equations. The equations fit the simulation results very well for α=40, which is a typical value. The performance decreases for more extreme cases where α is very large or very small.

The empirical equations developed in this section assume that the wave force is approximately linear with respect to wave height as shown in the previous section. These equations will be valid even if the wave force model changes as long as the new model does not deviate significantly from the linearity assumption.

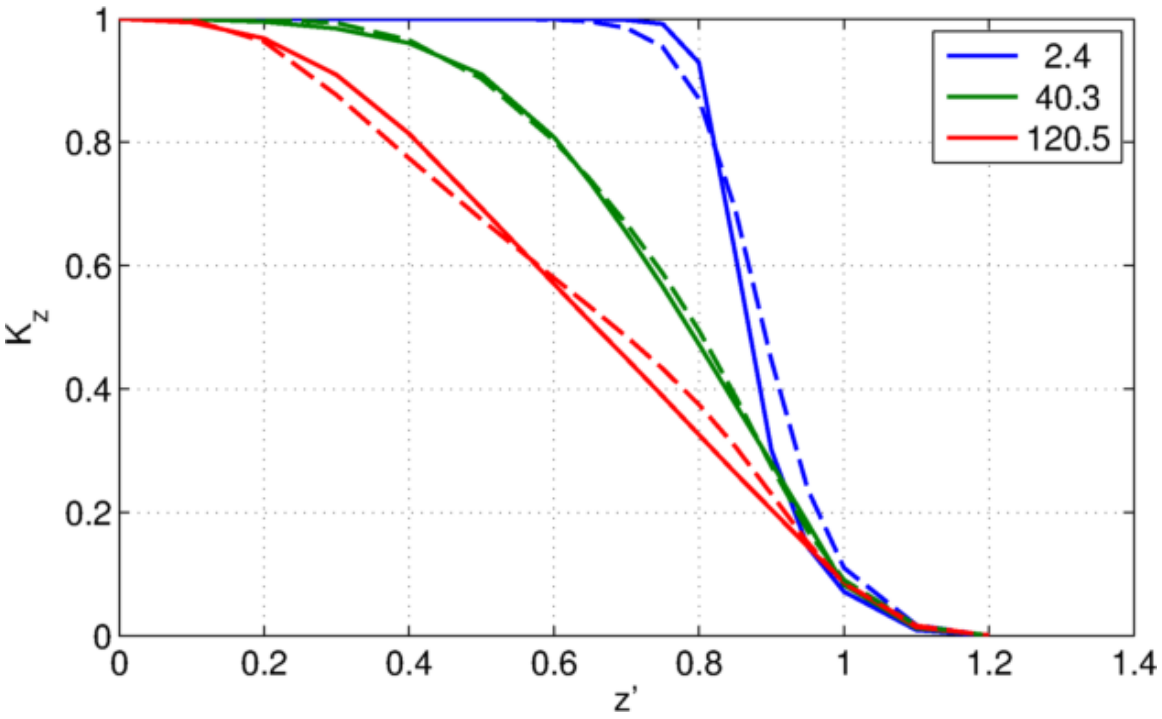

Figure 8-11 K_z as a function of z'. Legend shows α. Solid lines are simulations and dashed lines are the empirical equations.

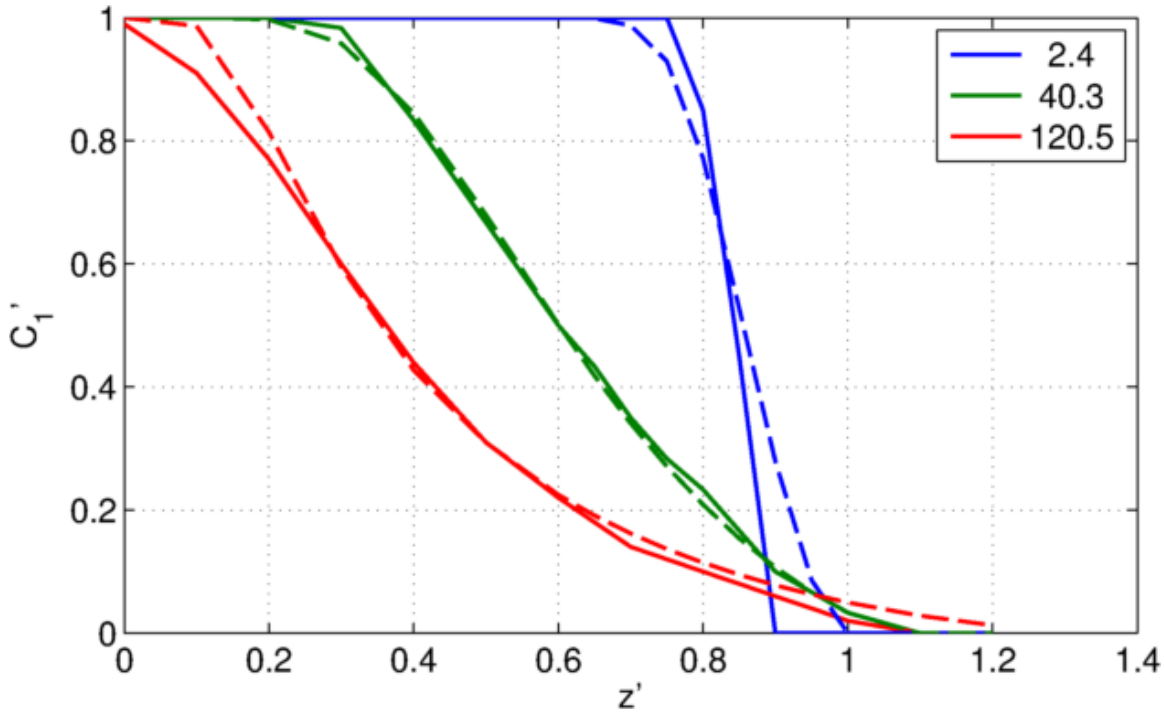

Figure 8-12 C_1' as a function of z'. Legend shows α. Solid lines are simulations and dashed lines are the empirical equations.

9.0 Application of the Equations for Different Levels of Met/Ocean Information

The predictive equations are a function of span length, L_s, wave length, l, clearance, z_c, significant wave height, H_s, and directional spreading, D_{spr}. All of these parameters except D_{spr} are already required for wave force calculations. Methods of predicting D_{spr} for different levels of available met/ocean information are discussed in this section. The AASHTO code for storm surge and wave loads on bridge superstructures, "*Guide Specifications for Bridges Vulnerable to Coastal Storms"*, outlines three different levels of analysis for obtaining the met/ocean conditions required to compute storm surge and wave loads on bridge superstructures. These levels are defined as Levels I, II, and III and the amount of effort required and the accuracy increase with level.

9.1 Level I Met/Ocean Analysis

For a Level I analysis the wave parameters, H_s and T_p are predicted using the empirical equations in the USACOE Shore Protection Manual. Directional wave spectra are not predicted. Attempts to find a correlation between D_{spr} and H_s, T_p and location (i.e. different shaped water bodies, etc.) proved to be futile as can be seen in Figure 9-1. This suggests that D_{spr} is more a function of the hurricane properties and path. In the absence of directional wave spectra it is recommended that the conservative value of 15 degrees be used.

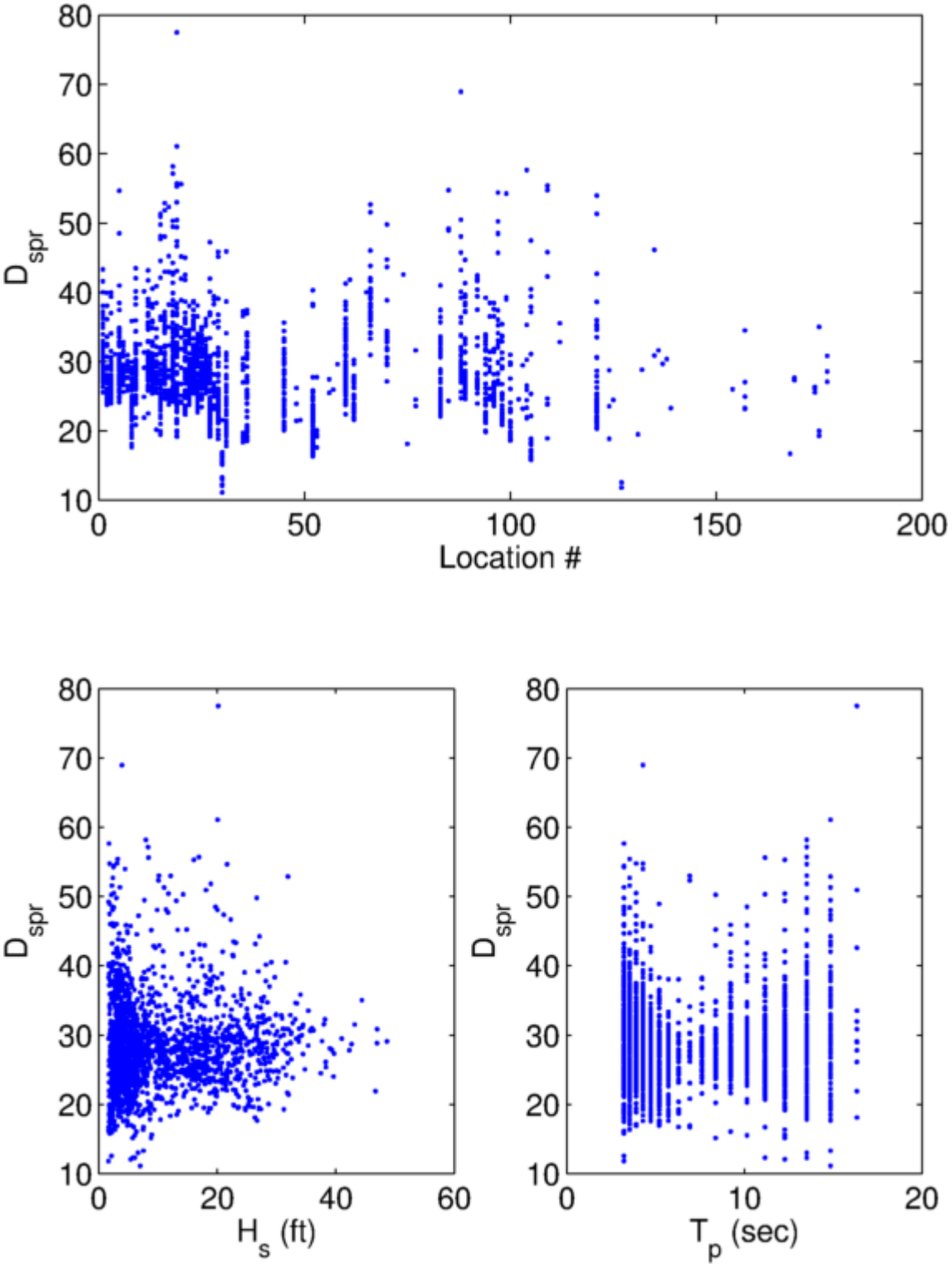

Figure 9-1 Directional Spreading, D_{spr} as a function of location, H_s and T_p.

9.2 Level II Met/Ocean Analysis

Limited wave modeling has been performed at this level. Usually winds at a given wind speed and various directions have been simulated. D_{spr} associated with the chosen wind direction should be used in wave force predictions. However, since the wind speed and direction is constant in these simulations, this will, in general, produce small values for D_{spr} which will result in conservative force predictions.

9.3 Level III Met/Ocean Analysis

In a Level III analysis the most significant tropical storms and hurricanes that have impacted the area of interest have been hindcasted and extreme value analyses performed on the met/ocean parameters. With the quantity and quality of information available from the Level III analysis a number of options are available for predicting the design D_{spr}. The easiest method is to use the smallest value of D_{spr} produced by the 10 storms with the closest H_s value to the 100-year value computed for the site. That is, pick the 10 storms (from those hindcasted) that produced significant wave heights closest to the 100-year significant wave height computed by the extreme value analysis for that site and pick the smallest value of D_{spr} produced by the 10 storms for that site for the force computations.

The above approach is sufficient for most situations but information from a Level III analysis does exist that allows a more sophisticated analysis of the surge/wave forces. In this approach the surge/wave forces are computed for all of the hindcasted storms and the extreme value analysis performed on the forces. In this way the forces for different frequency events can be determined. This assumes, of course, that there are a sufficient number of storms producing forces on the span to produce statistically significant results from the extreme value analysis.

An even more sophisticated and accurate approach is using direct sea surface simulations rather than the empirical equations developed based on these simulations. Direct simulations can also include depth limitations and steepness limitations in the calculations of C_0.This approach will be examined in the next section.

10.0 Field Test for the Methodology

Hurricane Ivan imparted significant damage to the bridges on Interstate 10 over Escambia Bay in 2004. A hindcast of Hurricane Ivan was performed by OEA as part of BHR for the replacement bridges. The FDOT compiled significant damage information on the existing bridges and this coupled with the hindcast data was used to test the surge/wave force predictive equations developed as part of the FHWA-AASHTO study. The most significant unknown in the predictive equations is the amount of entrapped air between the girders. The two limiting cases, 0% and 100%, were analyzed. If the actual amount was somewhere between these limits, then the predictive equations did a good job in predicting both the spans that failed and those that survived.

This dataset remains the best available for testing surge/wave force predictive methods. However, there have been significant improvements in storm surge and wave models and modeling techniques since 2004, so the decision was made to hindcast Hurricane Ivan once again for this study. The tightly-coupled ADCIRC-SWAN model was used. This provided improved water levels, significant wave heights and directional wave spectra at the bridge site and throughout the area.

Figure 10-1 shows the extent of the model mesh. The mesh contains bathymetry interpolated from NOAA datasets for both nearshore (coastal relief data set) and open ocean (ETOPO2, ETOPO5) regions and U.S. Army Corps of Engineers (USACE) surveys. The mesh covers the western North Atlantic Ocean, the Gulf of Mexico, and the Caribbean Sea. The mesh includes more than 79,000 triangular elements with over 42,500 nodes located at the corners of the elements. Multiple sources provided the data to refine the constructed mesh. The 2006 aerial LIDAR data specified the land boundaries and topography near the bridge. Figure 10-2 shows the peak water surface elevations at the bridge site and covers Escambia Bay, Pensacola Bay, and the East Bay.

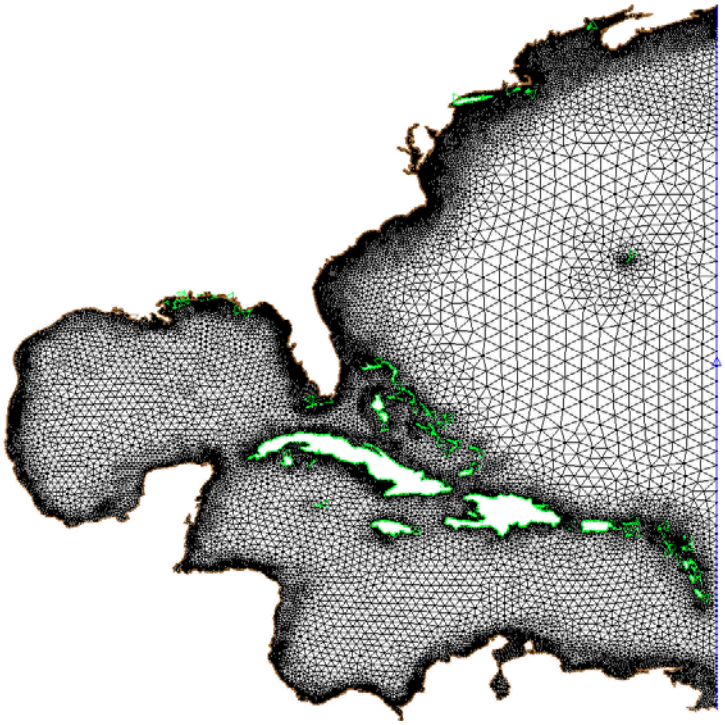

Figure 10-1 Extent of ADCIRC/SWAN mesh

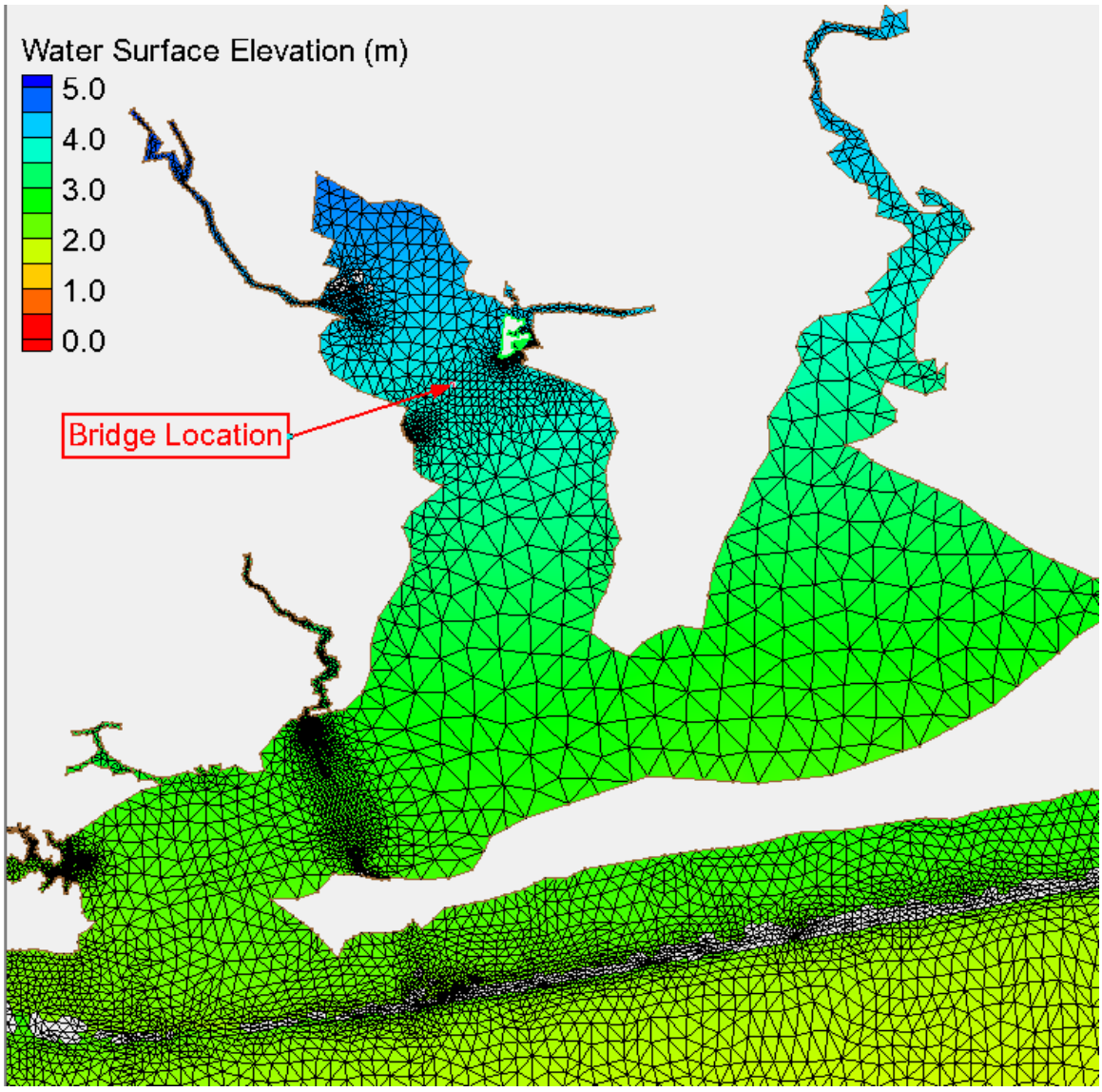

Figure 10-2 Contour map of peak water surface elevation at bridge location

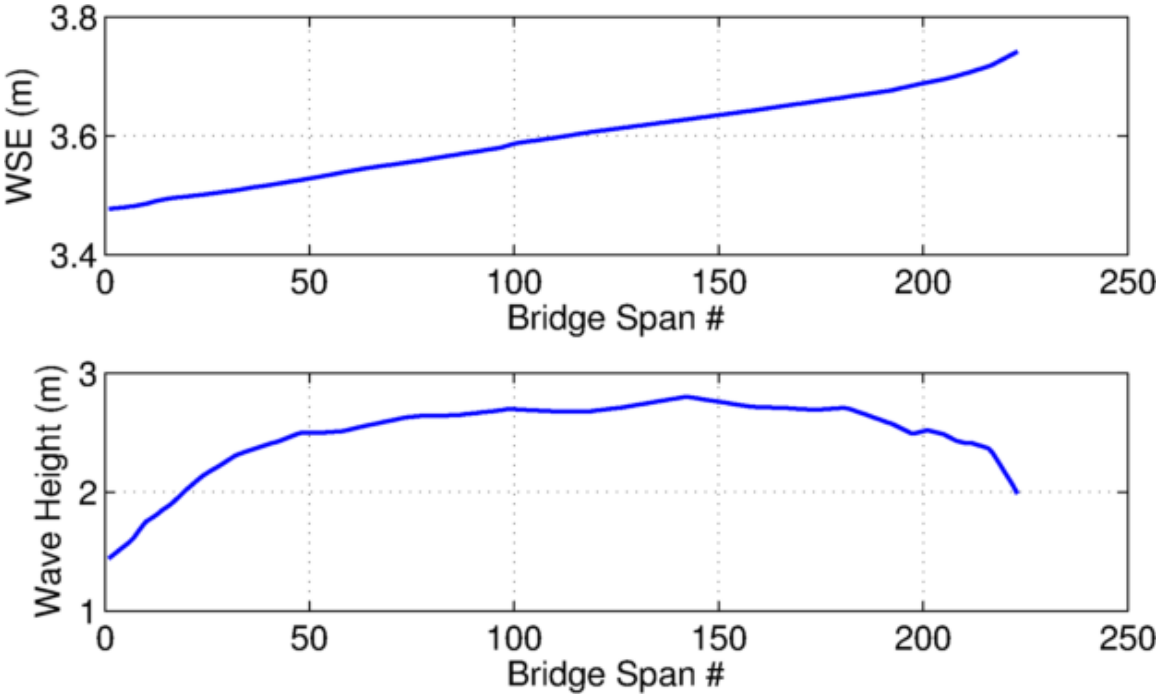

Figure 10-3 Maximum water surface elevation and associated significant wave heights at the bridge spans.

The maximum water surface elevation and associated significant wave heights at the bridge spans are shown in Figure 10-3. These values were used in the wave crest length and surge/wave force calculations. The D_{spr} and α parameters are plotted in Figure 10-4. D_{spr} varies slightly across the bridge decreasing slightly at both ends. The large changes in bridge span lengths are the major cause for the variation in α along the bridge. Figure 10-5 shows C_0 calculated using the empirical equations with (green line) and without (blue line) the SF_E factor and with direct sea surface simulations using SWAN wave spectra (red line). Solid curves show SF_M=1 and dashed lines show SF_M=1.3. Normally, steepness effects are taken into account when creating sea surfaces, but since those effects were not taken into account in the development of the empirical equations for C_0, direct simulations, excluding steepness effects, are shown. For the case of SF_M=1 the empirical equations are a good fit to the data created by the simulations. Including the safety factor results in a conservative prediction that envelopes all of the simulation results. However, when SF_M=1.3 the empirical equations are about 3% less than the simulations even with SF_E=1.2. The large change in α is not reflected in the C_0 values since the long spans with large α are elevated and their low-chord are above the wave crests. The value of C_0 for the spans reached by the waves is around 1.70 compared to the default value of 1.8.

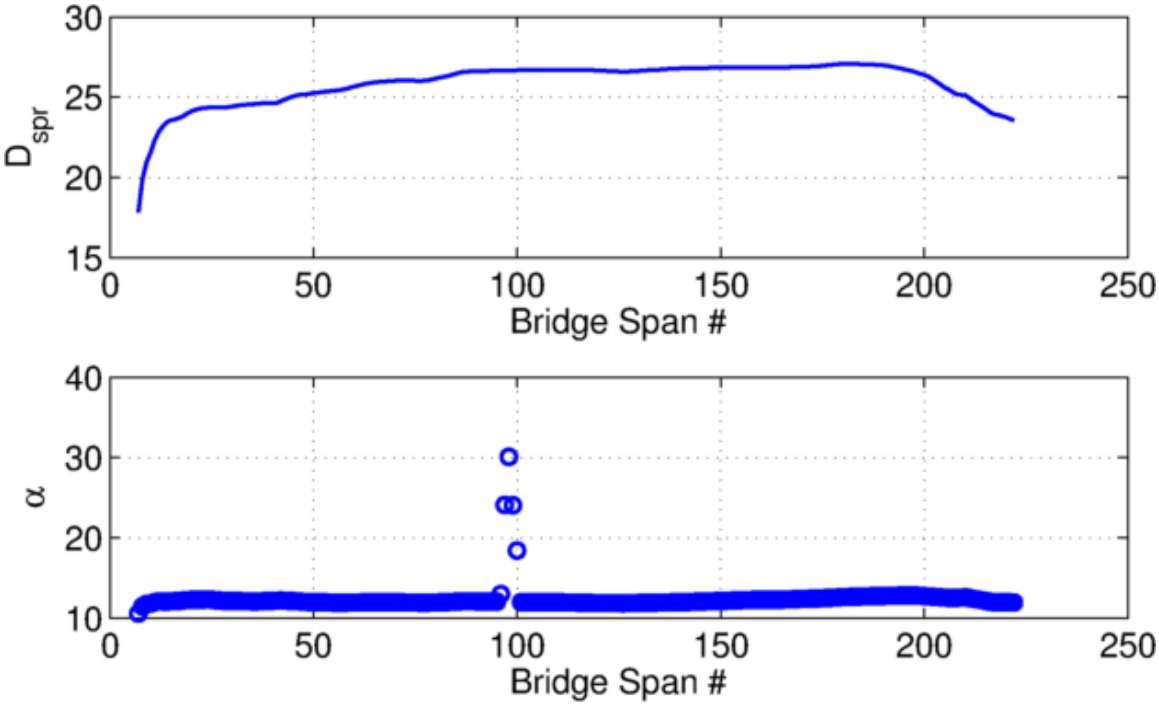

Figure 10-4 Directional spreading parameter and α computed using the empirical equations.

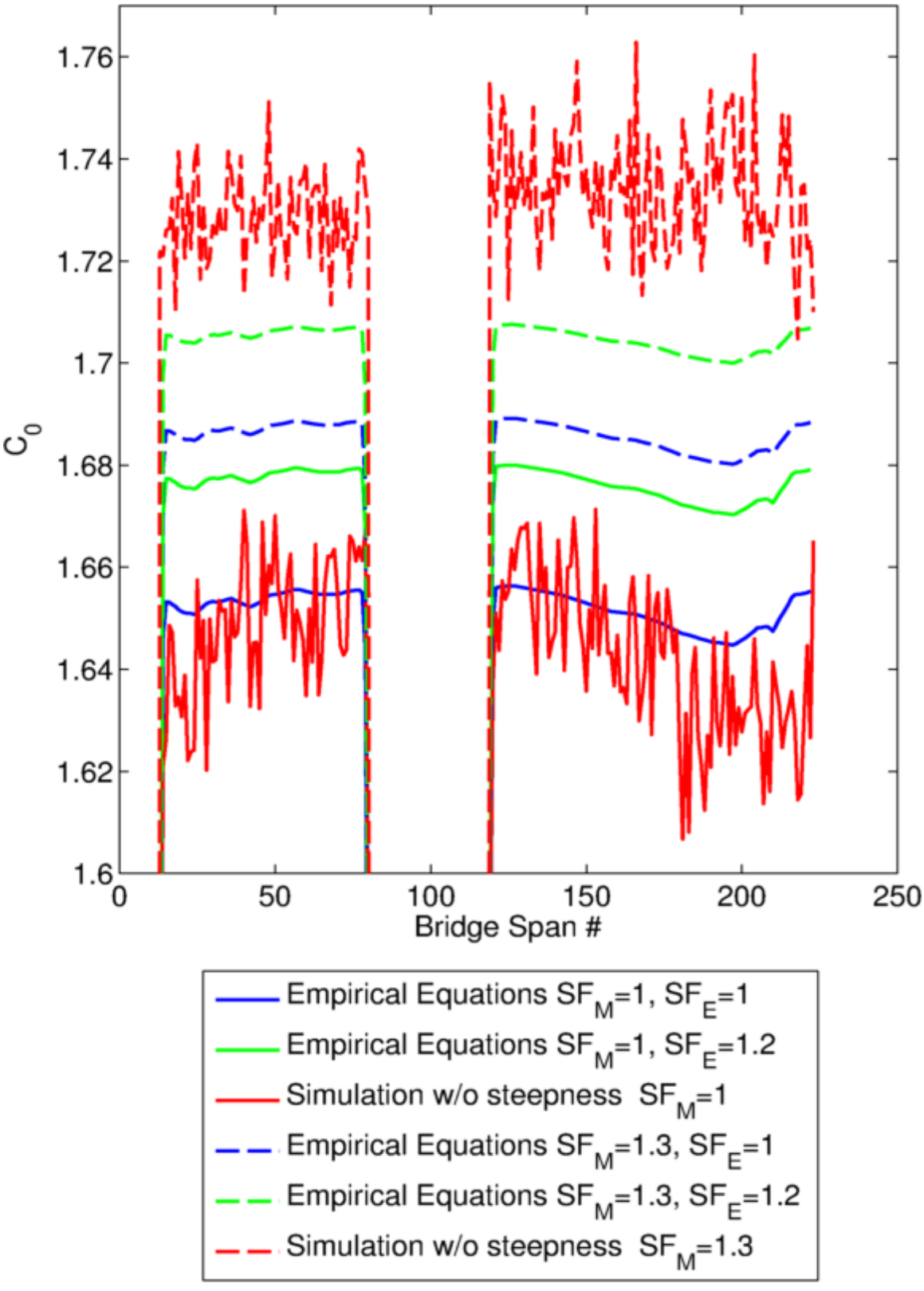

Figure 10-5 Parameter C_0 calculated using empirical equations and direct sea surface simulations.

The C parameters are compared in Figure 10-6. The steepness limitation is controlling the empirical equation results. As a result SF_E does not have an effect on C, therefore the blue and green curves overlap.

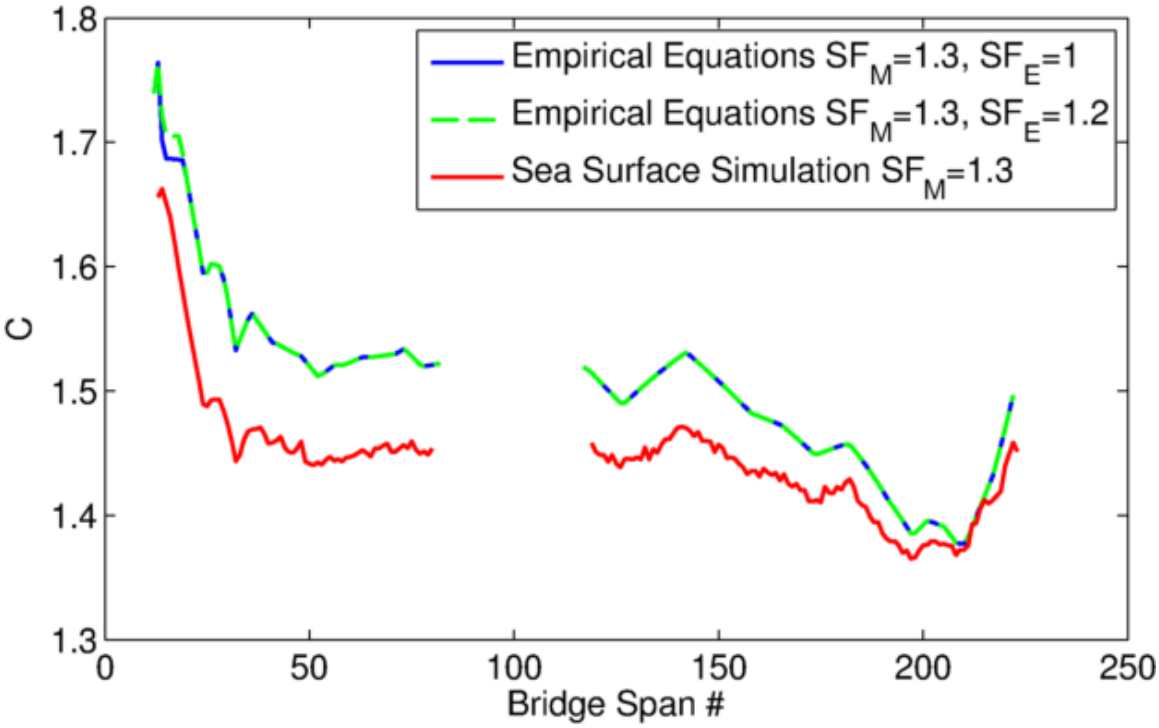

Figure 10-6 Parameter C calculated using empirical equations and direct sea surface simulations.

Wave forces consist of a quasi-static portion and a slamming portion. There are different equations for slab and girder type spans for quasi-static equations, but there is only one equation for slamming forces and it is based on slab type spans. This gives very conservative results for girder type structures as the I-10 Bridge. For girder structures it is estimated that the slamming force magnitude is approximately 20% of that for an equivalent size slab structure. This needs to be verified by analyzing pressure data obtained from the air spaces between the girders during laboratory tests.

The resulting vertical wave forces are compared in Figure 10-7. The solid lines show the forces calculated using sea surface simulations and PBM. The calculations based on empirical equations for 3D sea surface effects and parametric wave force equations are shown with dashed lines. The failure patterns of the spans are within the two limiting cases examined: 0% air entrapment and 100% air entrapment, showing that the new methodology was successful in this field test application. The conservative empirical + parametric equations are 40% larger than the more accurate simulation method. However the equations are slightly less than the simulations for 0% air. However it should be noted that AASHTO code does not advise using 0% air entrapment and this value will not be used in applications.

The new method for calculating 3D sea surface effects does not decrease the wave forces for this case because wave steepness criteria are controlling the final result. In the Figure 10-5 dashed green curve C_0 is around 1.7 (compared to a standard value of 1.8). Since wave forces are linear with wave height, the reduction in wave forces in the absence of steepness effects is around 5%. The reduction is very small as expected since the span lengths are very small. If the span lengths had been 160 ft the reduction in wave forces would be 14%. However for longer spans, shorter wave periods and/or smaller directional spreading wave forces can decrease as much as 50%.

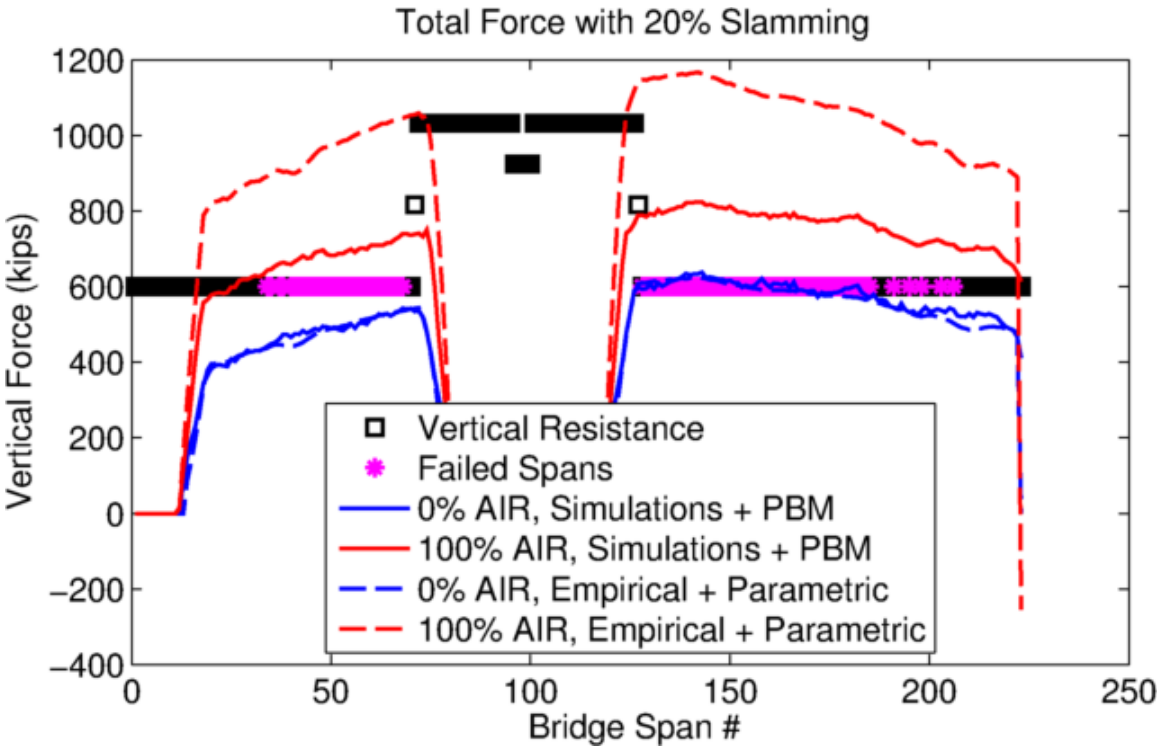

Figure 10-7 Predicted vertical forces at I-10 Escambia Bay Bridge.

11.0 Summary and Conclusions

Wave forces on bridge superstructures are dependent of the variation in design wave crest height over the length of the bridge span. In the AASHTO code, it is assumed that the wave crest elevation is unchanged and extends the length of the span regardless of the span length. The purpose of this research project was an attempt to quantify wave crest lengths in enclosed coastal waters under tropical storm and hurricane conditions. Since wave crest heights vary along the crest, it is necessary to define a threshold height above the storm water level to establish the crest length (Figure 8-1). Attempts to arrive at a meaningful way to set the threshold height were not successful. This, however, provided motivation for the development of a method for accounting for wave crest variation and its impact on wave forces on bridge spans without defining a threshold value. This method takes into consideration both the length of the span and the distance between the storm water and the span low-chord elevations. Methodologies for obtaining design wave height and period based on the met/ocean information that is available is presented. When directional wave spectra for the major storms that have impacted the location of interest are available (e.g., a Level III met/ocean analysis has been performed and the spectra saved), more accurate design wave heights and periods can be obtained. For situations where wave spectra are not available (Level I met/ocean analysis), conservative values for the spectral parameters must be used that result in conservative force estimates. However, for longer span lengths the methods developed in this study will result in reduced predicted wave loads even when limited met/ocean data is available. Additional research on design wave periods in steepness-limited cases, and slamming forces for both slab and girder bridge superstructures, will significantly improve the accuracy of predicting wave loading on bridge superstructures.

References

Forristall, G. Z. (2000). "Wave crest distributions: Observations and second-order theory." *Journal of Physical Oceanography*, 30(8), 1931–1943.

Goda, Y. (1994a). "Statistics of wave crest lengths based on directional wave simulations." *Journal of Offshore Mechanics and Arctic Engineering*, 116, 239.

Goda, Y. (1994b). "Statistics of Wave Crest Lengths Based on Directional Wave Simulations." *Journal of Offshore Mechanics and Arctic Engineering-Transactions of the Asme*, 116(4), 239–245.

Goda, Y. (1999). "Numerical simulation of ocean waves for statistical analysis." *Marine Technology Society Journal*, 33(3), 5–14.

Longuet-Higgins, M. S. (1963). "The effect of non-linearities on statistical distributions in the theory of sea waves." Journal of Fluid Mechanics, 17(03), 459–480.

Modjeski and Masters, Inc., Moffatt and Nichol, Inc., Ocean Engineering Associates, Inc., and Mertz, D. R. (2008). Guide Specifications for Bridges Vulnerable to Coastal Storms. AASHTO.

Monaldo, F. M. (2000). "Measurement of wave coherence properties using spaceborne synthetic aperture radar." *Marine structures*, 13(4-5), 349–366.

Romero, L., and Melville, W. K. (2011). "Spatial Statistics of the Sea Surface in Fetch-Limited Conditions." *Journal of Physical Oceanography*.

Sharma, J. N., and Dean, R. G. (1979). "Development and evaluation of a procedure for simulating a random directional second order sea surface and associated wave forces." University of Delaware.

Tucker, M. J., Challenor, P. G., and Carter, D. J. T. (1984). "Numerical simulation of a random sea: a common error and its effect upon wave group statistics." *Applied Ocean Research*, 6(2), 118–122.